Parametric analysis of RSB sensors for concrete strength monitoring using hybrid EMI and WP techniques: Numerical investigation

Moinul Haq [a,*], Adnan Khan [a], Tabassum Naqvi [a], Mohammad Yusuf [b,*], Hesam Kamyab [c,d,e], Shreeshivadasan Chelliapan [f,*]

[a] Department of Civil Engineering, Zakir Husain College of Engineering and Technology, Aligarh Muslim University, Aligarh 202002, India
[b] Institute of Hydrocarbon Recovery, Universiti Teknologi PETRONAS, Bandar Seri Iskandar, Perak 32610, Malaysia
[c] Faculty of Architecture and Urbanism, UTE University, Calle Rumipamba S/N and Bourgeois, Quito, Ecuador
[d] Department of Biomaterials, Saveetha Dental College and Hospital, Saveetha Institute of Medical and Technical Sciences, Chennai 600 077, India
[e] Process Systems Engineering Centre (PROSPECT), Faculty of Chemical and Energy Engineering, Faculty of Engineering, Universiti Teknologi Malaysia, Skudai, Johor, Malaysia
[f] Engineering Department, Razak Faculty of Technology & Informatics, Universiti Teknologi Malaysia, Jalan Sultan Yahya Petra, 54100 Kuala Lumpur, Malaysia

ARTICLE INFO

ABSTRACT

The strength of concrete after its casting increases with time up to a certain limit due to continuous hydration reactions in the cement matrix. To measure the rate of strength development and ultimate capacity of concrete, a novel health monitoring method using Reusable smart bolt (RSB) piezoelectric sensor is proposed in the present paper. The smart piezoelectric Lead zirconate titanate (PZT) patch-based Electro-mechanical impedance (EMI) and Wave propagation (WP) techniques are utilised for accessing the health of concrete at 1, 3, 5, 7, 14, 21 & 28 days of concrete hydration. Firstly, the PZT patch-based sensing capabilities are validated with the experimental results from literature by modelling concrete cube for EMI and beam for WP results. Then, a total of 31 finite element models of concrete cubes having different RSB configurations were taken into consideration for sensor design and optimization. In EMI technique, the shifting of conductance signatures and relative resonance frequency are measured, whereas in WP technique, the shift of P-wave velocity peaks between actuator and sensor is estimated for all the models. The sensitivity of outputs is measured by plotting statistical Root mean square deviation (RMSD) index which proven the efficacy of employing RSB sensors for monitoring concrete strength-development during early-hydration ages with good correlations. Overall, the EMI-identified RMSD plotted for conductance shows 327 % more sensitivity than WP-identified relative change of P-wave velocity in monitoring concrete strength development using RSB sensors.

1. Introduction

To assure structural integrity and safety, Structural health monitoring (SHM) intends to develop automated systems for detecting and estimating damages in structures. An effective SHM system can diagnose damages in real-time conditions using measured strains, stresses, pressures, temperature variations etc. It mainly comprises three parts: a sensor, a data-processing system (which includes data gathering, transmission, & storage), and a health prognosis system (which includes diagnostic tools and data management). Beside damage prognosis, monitoring the rate of strength development during hydration stages in fresh and hardened concrete is essential to dodge the structural failure

conditions. These failure conditions may occur due to non-attainment of design concrete strength at particular age because of bad workmanship, incomplete hydration, corrosion or de-bonding of steel rebars, shrinkage cracking. Estimating the real-time concrete strengths during very-early (0–1 day after casting), early (1–28 days), and later (more than 28 days) hydration stages ensure safety while predicting remaining life of structure in working conditions. Nowadays, sensors made up of smart materials such as fibre optic sensors [1,2], piezoelectric sensors [3,4], magneto-strictive sensors [5,6], shape memory alloys [7,8], acoustic emission sensors [9,10], self-diagnosing fibre-reinforced structural composites [11,12], magneto-rheological fluids [13,14] have shown tremendous capabilities in sensing various mechanical characteristics
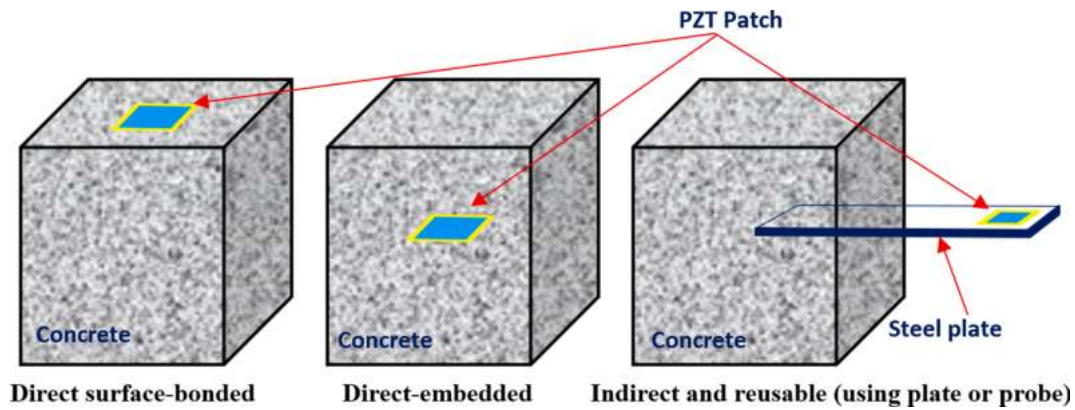

Fig. 1. PZT patch bonding configurations used for monitoring health of concrete host.

pertaining to the structural health. One of them, the piezoelectric material based smart ceramic patches made of Lead Zirconate Titanate (PZT) has gained attraction for diagnosing the health of civil structures in last two decades.

PZT sensors emerge as an active-sensing method based on detecting Electro-mechanical impedance (EMI) or elastic Wave propagation (WP) responses. A number of methods have been put forth to draw the PZT-structure interaction generally [15–23]. The static approaches were the initial efforts, followed by the various dynamic approaches demonstrated by various researchers. Crawley and Luis [15] presented static evaluations for several piezoelectric actuator models that led to comprehensive analytical solutions. Both completely bonded and finite bonding layer models for the surface-bonded instances were given and compared analytically and experimentally. A basic model by Liang et al. [24], having PZT actuator-driven 1-D spring-mass-damper system, was used in coupled analysis that demonstrated estimation of actuator power consumption and energy flow in coupled electro-mechanical systems. A system-identification model of piezo actuators for induced-strain excitation of 2D active structures was presented by Zhoe et al. [25] which acted as an improvement over 1-D model. Bhalla and Soh [26] proposed a further adjustment and enhancement in modelling by including the definition of effective impedance while taking into account the force transfer distribution throughout the whole boundary of the PZT patch. Based on the effective impedance, Wang et al. [27] developed a 3D EMI model that describes the interaction between an implanted square PZT transducer and the host structure. In EMI technique, a PZT patch attached to a structure is driven by a fixed, alternating electric field at higher frequency, causing a slight deformation in the PZT patch and the associated structure. The electrical reaction to mechanical vibration of that local region is transmitted back to the same PZT patch. The electrical impedance response changes when a crack or other damage alters the mechanical dynamic response. Therefore, by measuring the electrical impedance of the PZT patch, structural health can be indirectly monitored. On the other side, in WP technique, an ultrasonic elastic wave was propagated from the PZT patch acting as an actuator. The initial peak's amplitude and time of arrival were noted and examined for another PZT patch acting as sensor. It is noted that a larger region can be monitored with an elastic wave-based technique than with an impedance-based one. Some other piezo sensors-based techniques include global dynamic technique, frequency response spectrum analysis, and model-shape based analysis. Apart of these piezo based techniques, some other concrete strength monitoring methods includes rebound hammer method, ultrasonic pulse velocity technique, core-drilling methods, nail-shooting method, pull-out and pull-off methods [4].

Besides the conventionally used direct surface-bonded and embedded configurations of PZT patch for concrete health monitoring, there are various indirect reusable attachments such as magnetic

attachment, smart probe, bolted attachment used by researchers in the past studies [28–31]. The capacity of the PZT patch to be used repeatedly is referred to as "reusable". A Reusable smart bolt (RSB) sensor (*i.e.*, PZT patch indirectly attached to substrate through an additional steel bolt attachment), contrary to directly attached sensors which is made for single-use applications, may be detached or teared out from one substrate after a measurement and reattached to another substrate or at new location of the same for additional measurements. Due to its reusability, it can be used to monitor concrete strength development in a variety of situations without the requirement for costly sensor replacement. Utilising modified RSB configurations may increase the effectiveness of SHM, as additional indirect attachment acting as a protective device for PZT patch is not in direct contact with harsh concrete environment. Moreover, additional attachment enables simple installation and removal of patches without causing damage which may open the doors for its effective utilisation in actual concrete structures on a larger scale. However, on contrary, in some cases steel bolts of RSB sensors may experience fatigue, corrosion and other degradations that can compromise structural integrity and fluctuates the results. To overcome these limitations and avoiding unnecessary errors in output signals, conditions of steel bolts and PZT patch should be checked at regular intervals. Fig. 1 shows labelled diagram of direct and indirect configurations of PZT patch bonded to concrete cube for SHM.

Various experimental studies to obtain the PZT patch based EMI and WP responses at different time of concrete hardening were demonstrated by researchers [32–38]. Wang and Zhu [36] uses asphalt lacquer coating to PZT patch to safeguard water contact while diagnosing concrete's strength gains during its curing duration. The Root-mean square deviation (RMSD) & Mean-absolute percentage deviations (MAPD) were correlated with strength gain to find the feasibility of EMI technique. Apart of evaluating impedance changes, the resonant frequency shifts of impedance peaks were monitored and correlated with elastic modulus of concrete during curing by Guo and Sun [37]. Later, Talakokula et al. [35] investigated the PZT patch-identified Equivalent structural parameters (ESPs) using EMI technique and found that stiffness and damping has better correlations with degree of hydration than RMSD. The successful application of PZT patch based WP techniques for concrete hydration monitoring was discussed by [20,39–41]. In a recent experimental study by Tang et al. [20], linear correlation was proposed between EMI and WP outputs for embedded PZT patch-based concrete strength development monitoring during hydration. Previously, the practical issues regarding concrete curing monitoring using WP techniques were discussed by [42]. In their study, it was concluded that a 5-peak sinusoidal tone burst actuated at 30–120 kHz as input signal with smooth & even patch bonding surfaces having 90 mm spacing between PZT transducers should be preferred for prominent results.

Despite having many experimental studies, due to the anisotropic nature of concrete, inhomogeneity, and other difficulties that are readily

caused during the concrete manufacturing process, the disparity in experimental testing outputs may be observed [43–45]. To understand the non-repeatable nature of PZT's output in case of concrete, various analytical studies were demonstrated for estimating strength gain during hydration phase [17,46–49]. The Finite element analysis (FEA) of PZT-structure interaction allows the computation of stresses and electric field distributions for different input conditions. It results in instantaneous evaluation of material characteristics and optimization of sensors parameters while dodging the difficulties arises during experimentation. In recent times, FEA also emerges as a potential tool for the EMI and WP technique simulations [50,51]. In the instance of EMI, numerical analysis was thought to be more effective and reliable than theoretical modelling [52]. Many studies proven SHM predictions effective using coupled field element analysis [27,49,53–55]. By simulating intricate geometry under critical loading conditions, numerical analysis allows a better understanding of the impedance effect. The dynamic interaction between strain-induced actuator & host structure was demonstrated by [1,51,56]. In an study by [57], it had been proven that numerical analysis based admittance approach outperforms the static and dynamic approaches. The EMI simulation for both free piezoelectric sensor and one-dimensional beam structure attached with the sensor showed closeness of numerically-obtained impedance signatures with the experimental ones [51]. Semi-analytical approaches that includes extracting eigenvalue and eigenvectors from numerical approach and then using them later in finding results of mechanical impedance was also demonstrated by [58]. The PZT FE-model based on the concept of 'effective impedance' was established to bridge the gap between 1-D and 2-D modelling [17]. In an another study, coupled field analysis was performed in ANSYS software by taking six damaged cases of concrete cube [59] while assuming it to be isotropic. The spectrum didn't follow the same trend as that of the experimental one. However, the deviations in RMSD value of the PZT patch attached near the damage area were higher. It was also observed that longitudinal mode impedance was less sensitive as compared to lateral mode.

The effect of adhesives can't also be fully neglected. Due to the shear-lag effect, the adhesive bond layer in between also has a significant impact on stress–strain transmission. A comprehensive derivation (semi-analytical) to include the shear-lag effect into impedance genesis, assuming pure shear deformation of the bonding layer was given by Bhalla and Soh [60] and was numerically modelled to study the stress–strain transfer mechanism by Moharana and Bhalla [61]. According to their parametric investigation, using a greater shear-modulus and a thin bond layer ensures precise strain transformation. Some authors analyzed the configuration considering this layer with host material as a spring-mass damper systems in their study [62–64]. Despite having various experimental studies on concrete hydration monitoring, very few have been conducted via. EMI and WP techniques. The PZT-concrete interaction during strength development phase of hydration is not known numerically, especially for different higher excitation frequencies. No study considering reusable smart bolt configuration for monitoring concrete strength during its hydration phase has been performed till date. Also, the optimization of the sensor's design has not been done yet for strength monitoring.

The research gaps stated above are been bridged in the present paper. At present, the integration of PZT patch-based WP and EMI approaches with monitoring the development of concrete strength is made due to its complementary nature. While WP technique offers insights into wave reflections and attenuation, suggesting the existence of flaws or changes in material characteristics, EMI enables the identification of continual interior structural changes, such as due to stiffness enhancement during hydration. Combining these methods gives engineers a more thorough understanding of how concrete develops its strength in real-time scenarios, enabling them to take proactive measures to protect the concrete's structural integrity and long-term durability. The numerical investigations are made to examine how the EMI & WP techniques can be used to measure the compressive strength of concrete in early ages of hydration (*i.e.*, from day 01 to day 28). Firstly, the validation of results with experimental values is made. Then, the efficacy of RSB sensor has been investigated for monitoring the strength development. The novelty arises in proposing design, modelling and analysing different types of reusable smart piezo bolts in order to extract the EMI and WP based outputs that are helpful for monitoring early-age concrete strength development. In comparison to studies carried out using direct PZT patch configurations for concrete strength monitoring and discussed in literature, the indirect configurations utilizing RSB sensors features low-cost, reusable and more effective SHM solution for concrete structures. Their designs are also optimized by evaluating the sensitivity of conductance signature using various statistical indices. The relationships and calibration charts are also proposed with higher accuracy for correlating the development of concrete's strength with RSB outputs. The forthcoming sections explore the theoretical-background and modelling perspectives of EMI & WP techniques present used in paper for SHM.

2. Theoretical background

In EMI technique, a PZT patch (bonded to host) is enforced by electric-voltage signals in user-defined frequency ranges to create mechanical strain. The structural responses, as of mechanical-strain in the substrate, is transformed back to the PZT patch through the electrical signals, in the form of impedance (or, inverse of it known as admittance) signatures. The EMI signature connects itself to the elastic properties of the host, which serves as a benchmark for strength assessment. It means that if the signature diverges from the baseline, there has been any phase diversification in the host material in vicinity of the sensor. Any variation in the physical characteristic of the host alters the obtained impedance response, which are matched to the pristine stage response for estimating the health.

Subsequent to its discovery by Liang et al. [16,65] in 1996, the EMI technique proves itself as a prominent SHM solution for civil & industrial infrastructure, as well as for medical sectors in last two-decades [66–68]. The Electro-mechanical admittance ($\bar{Y}$), in form of its real component termed as conductance (G), and an imaginary component termed as susceptance (B), is denoted mathematically as in Eq. (1) [68],

$$\bar{Y} = G + jB$$
$$= 4\omega \frac{l^2}{h} \left[\bar{\varepsilon}_{33}^T - \frac{2d_{31}^2 \bar{Y}^E}{1-\nu} \left(\frac{Z_{a,eff}}{Z_{s,eff} + Z_{a,eff}} \right) \left\{ \frac{1}{2} \left(\frac{\tan(C_1 \kappa l)}{C_1 \kappa l} + \frac{tan(C_2 \kappa l)}{C_2 \kappa l} \right) \right\} \right]$$

(1)

where, l & h refers to the half-length & thickness of PZT patch, ν be the Poisson's ratio, d_{31} is piezoelectric strain coefficient in d-31 mode of operation, ω is the angular frequency, $\boldsymbol{\varepsilon}_{33}^T$ ($= \varepsilon_{33}^T(1-\delta j)$) & $\boldsymbol{Y}^E$ ($= Y^E(1 + \eta j)$) refers to complexed electrical-permittivity and complex Young's modulus with η and δ be mechanical & dielectric loss factor of PZT patch, $j = \sqrt{-1}$, C_1 & C_2 be the PZT related correction factor, $k = w\sqrt{p(1-v^2)}/Y^E$ be the two dimensional-wave number, ρ be the PZT density, and $Z_{a,eff}$ & $Z_{s,eff}$ be the effective-mechanical impedance of PZT patch & substrate respectively. On the other side, the mechanical/structural impedance is defined as the push given per unit resultant velocity & is estimated as a function of stiffness, mass, damping (*k-m-c*). In present study, the two different statistical indices *i.e.*, Root mean square deviation (RMSD) index, & Relative resonant frequency (RRF) shift are taken into consideration for estimating the changes in *G*-signatures output with strength development of concrete. Mathematically, RMSD and RRF for conductance peaks can be represented as by Eqs. (2) and (3).

$$RMSD\ (\%) = \left(\sqrt{\frac{\sum_{i=1}^{n} \left(G_i^u - G_i^{ref} \right)^2}{\sum_{i=1}^{n} \left(G_i^{ref} \right)^2}} \right) \times 100$$

(2)

Table 1
Parameters considered for model updating of concrete at different curing age.

Age (Days)	Elastics modulus (GPa) [76,77]	Density (kg/m³) [78]	Poisson's ratio [79]	Relative permittivity [76]
01	12.91	2384.8	0.296	7.63
03	20.78	2392.6	0.287	7.28
05	26.96	2401.8	0.264	6.20
07	30.81	2410.1	0.251	5.01
14	32.32	2442.8	0.238	4.15
21	35.34	2469.1	0.236	3.34
28	38.30	2494.9	0.235	7.68

$$RRF = \frac{Peak\ frequency\ at\ n^{th}\ day}{Peak\ frequency\ at\ day - 01(baseline)} \qquad (3)$$

where, G_i^u is conductance peak under investigation, G_i^{ref} corresponds to the peak taken as reference/baseline for i^{th} model.

Apart of EMI technique, the WP technique holds the same working principle as of ultrasonic nondestructive testing indicator measuring Ultrasonic pulse velocity (UPV) while utilizing two or more PZT transducers for studying the wave characteristics passing through the substrate. The WP approach was first designed to detect damages in metallic components [69]. It was then expanded to include damage measuring [70], hydration monitoring [28,41], and structural concrete strength monitoring [71–73]. In WP technique, one PZT patch acts as an actuator whereas the other remaining patches acts as sensors that receives the transferred mechanical vibrations and generates the output in form of an electrical signals. There are two components to the wave propagation

definitions. The wave's voltage excitation signal is the first component. The excitation signal, denoted by Eq. (4), is a 5-cycle sine-burst modulated by a Hanning window with $A = 100$ V, $f = 100$ kHz, and $N = 5$ are the appropriate values.

$$E = A[1 - \cos(2f\pi t/N)]\sin(2f\pi t)[t < (N/f] \qquad (4)$$

where, f, N, and A be the central frequency, peaks-count, & half voltage amplitude respectively. The upper surface of second PZT is attached to the second component, the wave observation probe.

In case of the PZT transducer attached to concrete host, these vibrations are transferred to the concrete matrix in the same way as in the EMI-PZT technique through the adhesive layer. Likewise, WP technique solves the issue of utilizing this technique on the concrete before loosening of its plasticity. For this reason, the method offers continuous hydration monitoring in early and later stages of setting in real-time conditions. It is expected that when the PZT transducer is surface-bonded on thick concrete structure, it will primarily excite surface-waves (Rayleigh wave), also called R-wave. The R-wave spreads along the concrete's surface and progressively drops in strength with depth from the surface. Simultaneously, a pressure wave also called P-wave - with a superior velocity will be stimulated. The R- & P- waves will spherically move all across the medium. The elastic vibration will be changed back to electrical signals when it reaches another patch that functions as a sensor, owing to the direct piezoelectric action. Time-of-Flight (TOF), which is the time elapsed between the P- or R- wave transmission from actuator to arrival at the sensing transducer is estimated. As the concrete gain stiffness, wave propagation is affected and is reflected in the form of change in amplitude of wave and TOF. Gu et al.

Table 2
Electrical and mechanical characteristics of PZT patch, epoxy and concrete.

Properties	Materials		
	PZT-5H	Epoxy	Concrete cube
Density, ρ (kg/m³)	7800	1250	2380
Dimensions (mm³)	$20 \times 20 \times 1$	$20 \times 20 \times 0.3$	$150 \times 150 \times 150$
Elastic modulus, E (GPa)	63	4	12.91
Poisson ratios, ν	0.35	0.36	0.20
Dielectric loss factor, δ	0.02	–	–
Isotropic loss factor, η	0.0169	0.05	0.03
Relative permittivity, e_r	$\begin{bmatrix} 1730 & 0 & 0 \\ 0 & 1730 & 0 \\ 0 & 0 & 1700 \end{bmatrix}$	3.6	8.0
Elasticity matrix, C_E (Pa),	$\begin{bmatrix} 1.24e11 & 7.51e10 & 7.50e10 & 0 & 0 & 0 \\ 7.51e10 & 1.24e11 & 7.50e10 & 0 & 0 & 0 \\ 7.50e10 & 7.50e10 & 1.09e11 & 0 & 0 & 0 \\ 0 & 0 & 0 & 2.10e10 & 0 & 0 \\ 0 & 0 & 0 & 0 & 2.10e10 & 0 \\ 0 & 0 & 0 & 0 & 0 & 2.25e10 \end{bmatrix}$	–	–
Piezoelectric constants, d (C/N)	$\begin{bmatrix} 0 & 0 & 0 & 0 & 5.84e-10 & 0 \\ 0 & 0 & 0 & 5.84e-10 & 0 & 0 \\ -1.71e-10 & -1.71e-10 & 3.74e-10 & 0 & 0 & 0 \end{bmatrix}$	–	–

Table 3
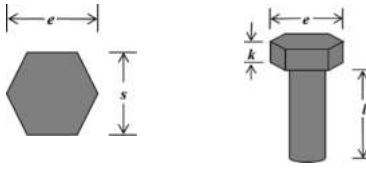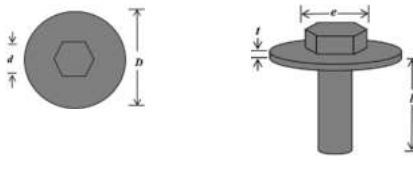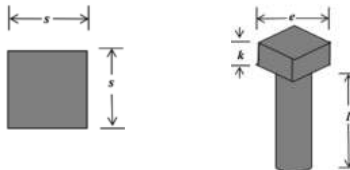Classification of bolt prototypes with dimension details considered in FE study.

Prototype-I Hexagonal head Bolt		Prototype-II Hexagonal head Bolt and washer		Prototype-III Squared head Bolt	
Top View	Isometric View	Top View	Isometric View	Top View	Isometric View
$s = 16$ mm, $k = 6.40$ mm (Specifications by ISO-4017)		$s = 16$ mm, $k = 6.40$ mm $D = 44$ mm, $d = 10$ mm, $t = 1.5$ mm (Specifications by ISO-4017)		$s = 16$ mm, $k = 6.40$ mm (Specifications by ISO-2585)	

Table 4
Nomenclature for different dimensions of bolt arrangement in RSB used for parametric study.

Dimension (mm)		Prototype I	Prototype II	Prototype III
l	35	PI-L35	PII-L35	PIII-L35
	70	PI-L70	PII-L70	PIII-L70
	100	PI-L100	PII-L100	PIII-L100
k	3.4	PI-H3.4	–	PIII-H3.4
	4.4	PI-H4.4	–	PIII-H4.4
	5.4	PI-H5.4	–	PIII-H5.4
	6.4	PI-H6.4	–	PIII-H6.4
d	8	PI-D08	–	PIII-D08
	10	PI-D10	–	PIII-D10
	12	PI-D12	–	PIII-D12
	14	PI-D14	–	PIII-D14
t	1.5	–	PII-WT1.5	–
	2.5	–	PII-WT2.5	–
	3.5	–	PII-WT3.5	–
D	44	–	PII-WD44	–
	49	–	PII-WD49	–
	54	–	PII-WD54	–

[71] proved the WP technique's capacity to track concrete strength development. Song et al. [74] carried out numerical and experimental demonstrations to reveal that a surface-bonded piezoelectric transducer system in concrete structures can generate and receive surface-wave propagations. Based on the FE analysis, it was concluded that piezo-electric actuator generated surface-waves can be easily recognized at significantly farther distances. Qin and Li [75] showed that the WP technique may be used as in-situ conditions with transducers embedded to monitor the hydration phenomenon at early-ages, as well as the health-condition of a concrete building after maturation. The hydration progress of cement was monitored using velocities estimations which were then used to compute the dynamic modulus of concrete.

On the other side, Finite element modelling (FEM) makes early idea evaluations simpler and reduces the need for and supply of physical prototypes. It also permits tests of a device's functionality and behaviour that are not possible in the real world. The best ideas for further study may be chosen much more easily with FEM. For instance, a superior RSB configuration would be considered for future experimental research out of the 31 variations examined in this article. From adopting one from the multiple ideas, it assists the researcher to make decisions-based design
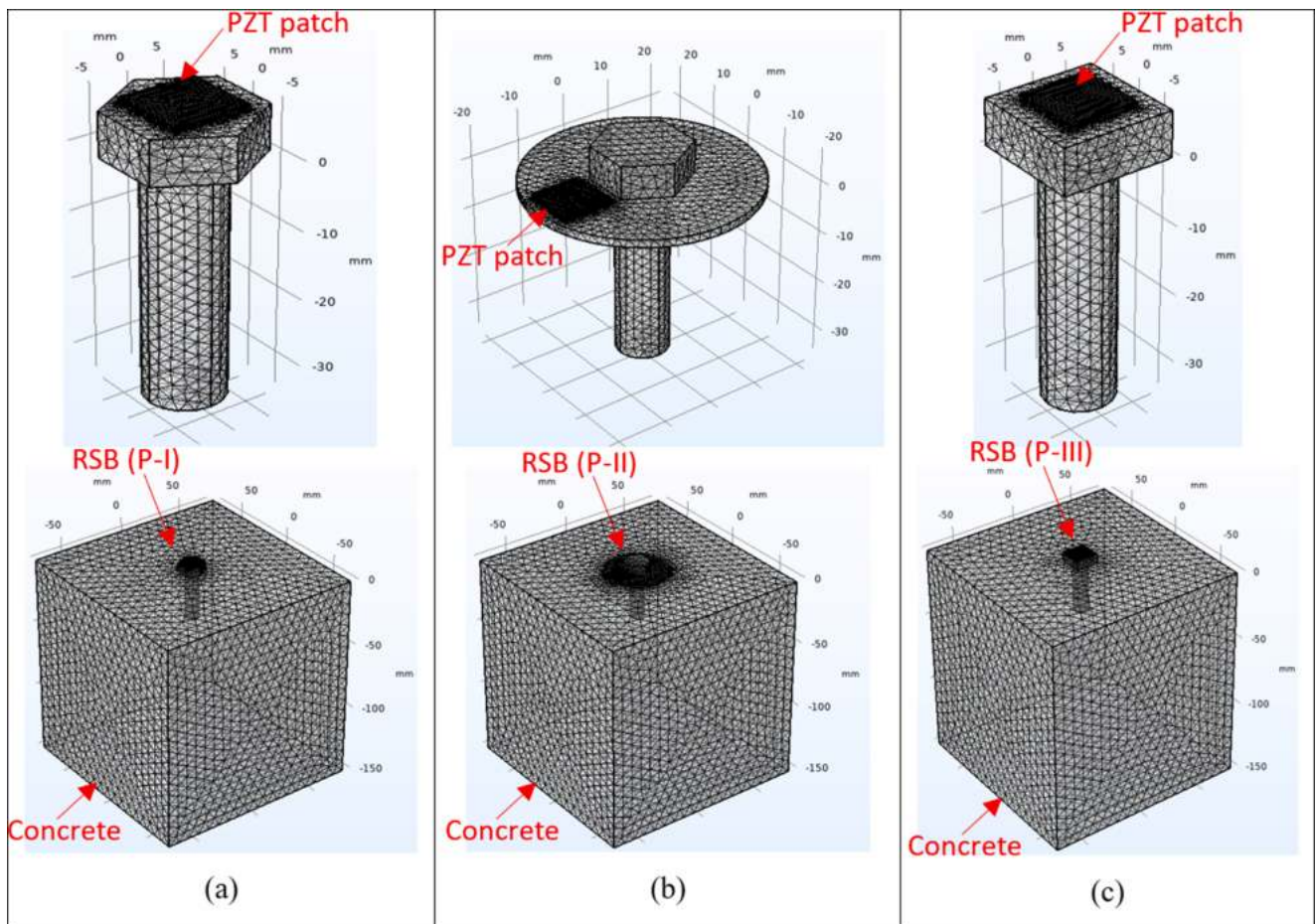

Fig. 2. Meshing of free and combined models of RSBs with concrete cubes (a) PI, (b) PII, and (c) PIII.

Table 5
Meshing statistics of FE concrete cube models with RSB considered in study.

Method	Configuration	Minimum element quality	Average element quality	Tetrahedron	Triangle	Edge element
EMI technique	PI-L35 (half model)	0.1498	0.6723	56,920	6178	531
	PII-L35 (half model)	0.1418	0.6723	61,030	7419	648
	PIII-L35 (half model)	0.1559	0.6692	56,477	6114	531
WP technique	PI-H6.4 (full model)	3.533E-5	0.6329	42,791	5691	724

Table 6
Meshing size of FE concrete cube models with RSB considered in study.

Method	Configuration	Maximum element size (mm)	Minimum element size (mm)	Curvature factor	Resolution of narrow regions	Maximum element growth rate
EMI technique	PI-L35 (half model)	8.65	0.629	0.4	0.7	1.40
	PII-L35 (half model)	8.68	0.632	0.4	0.7	1.40
	PIII-L35 (half model)	8.65	0.629	0.4	0.7	1.40
WP technique	PI-H6.4 (full model)	9.05	0.658	0.4	0.7	0.40
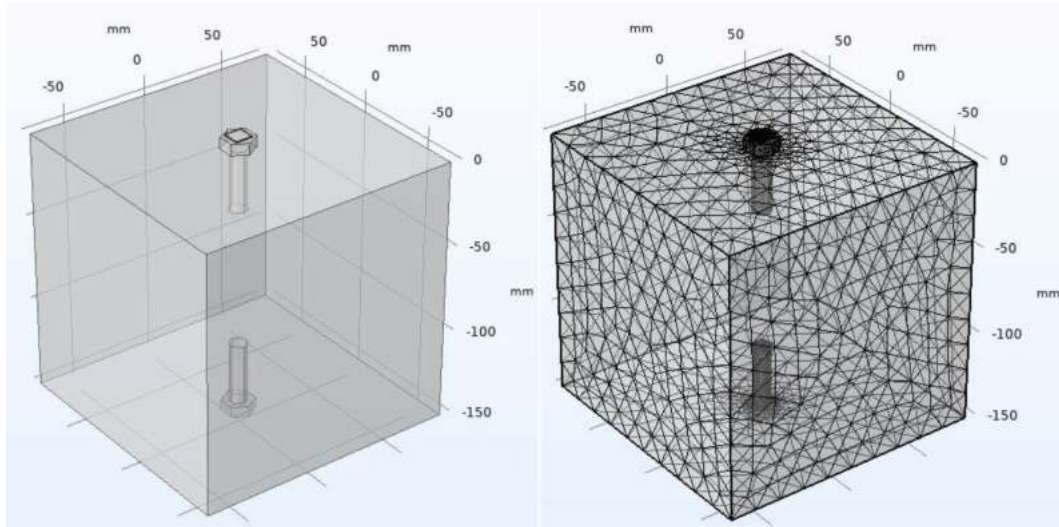
Fig. 3. (a) Isometric view of concrete cube modelled with RSB (PI-H6.4) on opposite faces, and (b) Mesh view of model.
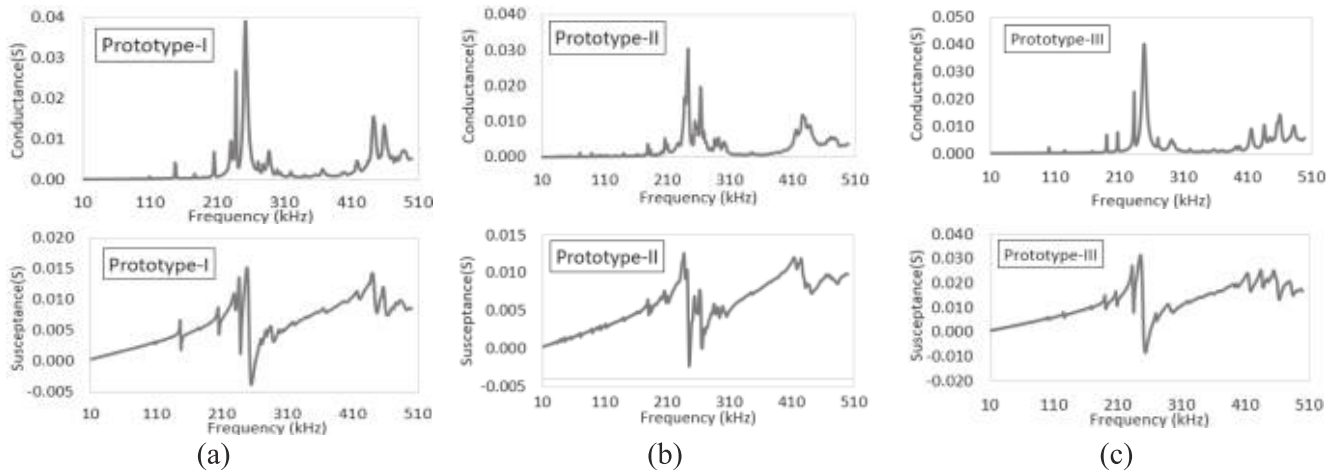
Fig. 4. Admittance response (in form of *G & B*) of free RSB prototypes (a) PI, (b) PII, and (c) PIII. (PZT excitation frequency ranges between 10 and 510 kHz).

on the information received as output from FEM. The development of concrete strength can be assigned by model-updating using the concrete properties at respective curing day from literature. At present, the strength evolution in concrete has been simulated by updating the density, Poisson's ratio, relative permittivity and elastic moduli of concrete with curing age as illustrated in Table 1 [76–80]. The concrete's compressive strength in its hydration phase is correlated to elastic moduli using Eq. (5) as adapted by [77] for various density depicted in Table 1.

$$E = 43\rho^{1.5}f_c^{0.5} \tag{5}$$

where, ρ, E, and f_c be the concrete's density, elastic moduli, and characteristic strength respectively. By using parametric assessments of tested models, FEA assists in extending already-concluded experiments outcomes. The ability to calculate and visualise a wide range of physical characteristics concurrently, as in the solid mechanics module's stresses or the electrostatic module's electric potential, enables developers to quickly assess performance and make any necessary adjustments later on. FEM lowers the cost of the experimental procedure to be carried out and speeds up the process of achieving a successful result. When it comes to structural health monitoring, it aids in the realistic modelling of loading circumstances and failure mechanisms that could be harmful, damaging, or unfeasible. The next section deals with numerically modelling and analysing the PZT based SHM system for strength development monitoring of concrete substrates.
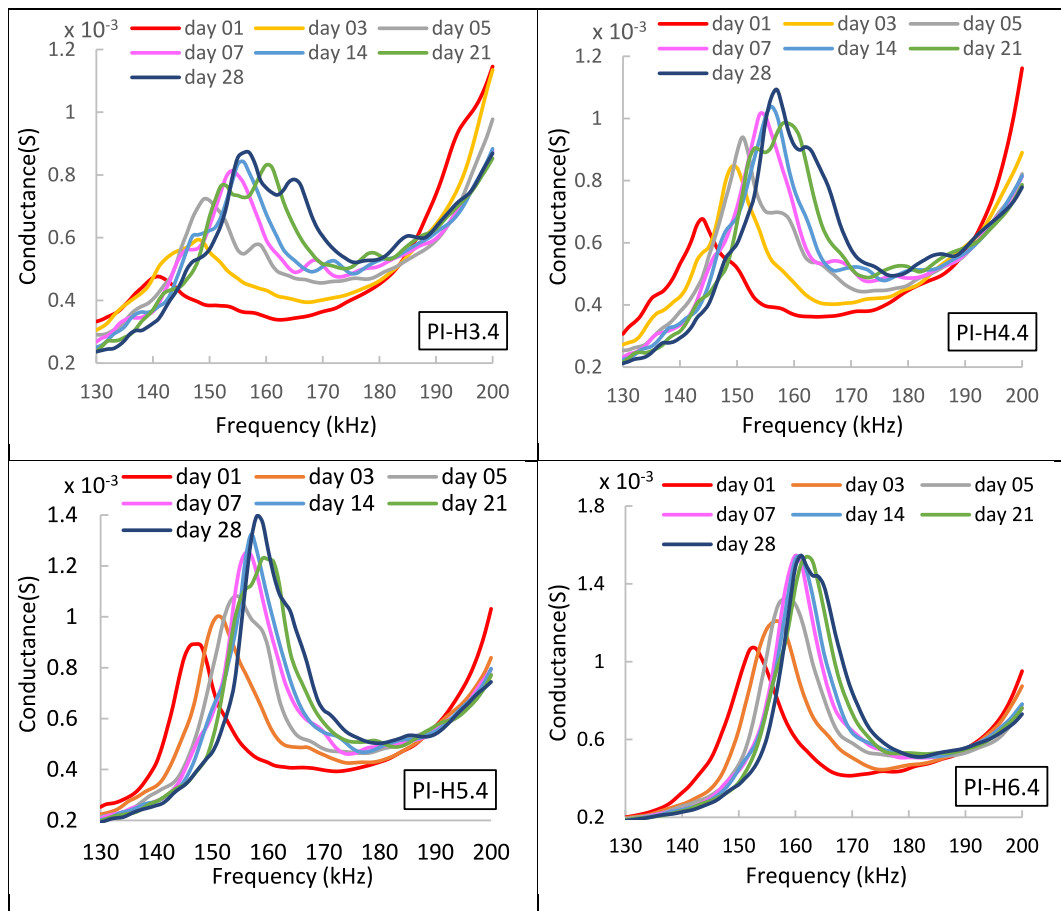
Fig. 5. Conductance signatures obtained at different concrete age upon altering bolt head thickness between 3.4 and 6.4 mm for Prototype-I.
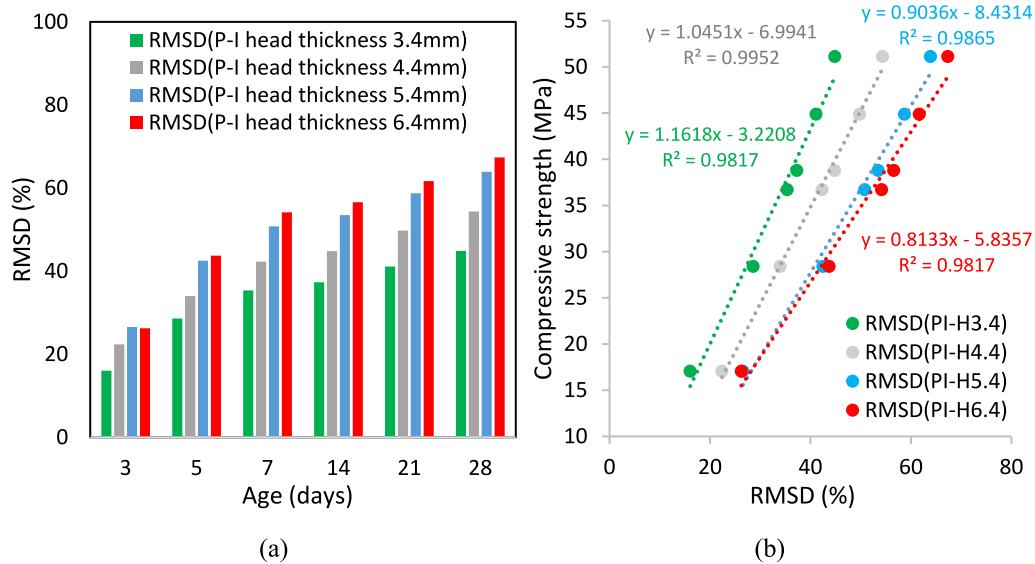

(a)   (b)

Fig. 6. (a) RMSD index of *G* for model PI on varying bolt head thickness and concrete age, and (b) Corresponding correlation between strength and RMSD for PI model.

3. Modelling concrete-PZT interaction with reusable smart bolt (RSB) configuration

A two-folds study has been worked out to demonstrate monitoring of concrete strength development numerically utilising PZT patch-based EMI and WP techniques. Firstly, the embedded configurations of PZT patch were considered for verifying numerically obtained results of both EMI and WP techniques with experimental ones (refer to Appendices) reported previously by [20,23]. Thereafter, 31 different RSB configurations were modelled and analysed to meet the objectives of present
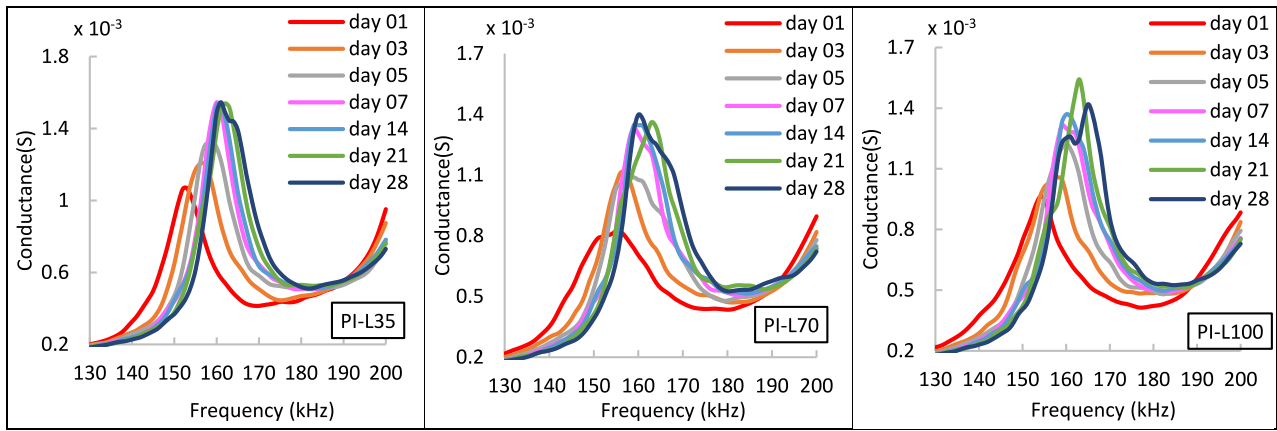
Fig. 7. Conductance signatures obtained at different concrete age upon altering shank length between 35 and 100 mm for Prototype-I.
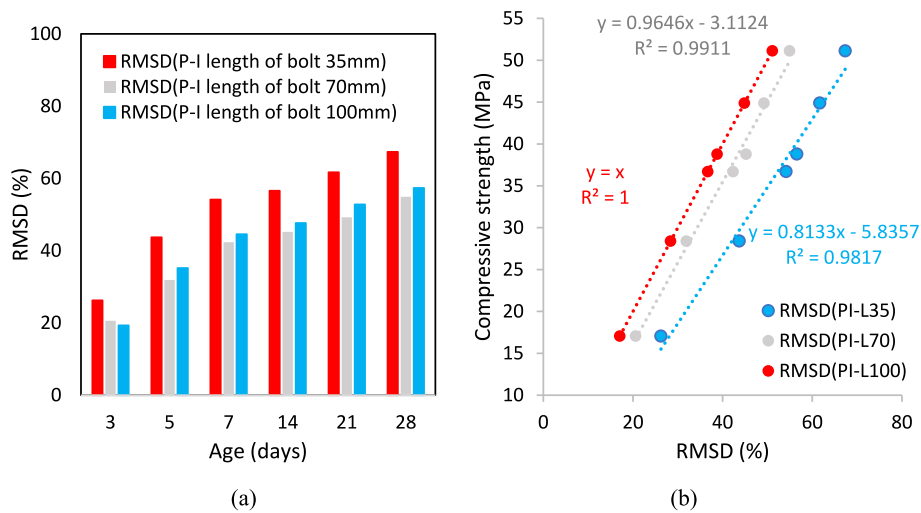

(a)

(b)

Fig. 8. (a) RMSD index of *G* for model PI on varying shank length and concrete age, and (b) Corresponding correlation between strength and RMSD for PI model.

study. For FE modelling, the properties of concrete and PZT are assigned to host and sensor respectively using finite element software namely COMSOL Multiphysics. The interfacial bonding layer of adhesive in case of embedded PZT configurations (used for verifications), is modelled at top and bottom face of PZT in order to glued PZT patch with the surrounding concrete, whereas in cases of RSB configurations, the bonding layer is modelled on bottom face for the purpose of connecting PZT patch with steel bolt. The electrical, mechanical and dimensional properties of the materials as depicted in Table 2 were implicated during modelling [3,17,81,82].

The coupled field analysis was opted to obtain the conductance response in EMI technique, and the wave propagation velocities in WP technique. The coupled field analysis entails comprehending the connection between the PZT patch's electrical impedance and the structure's mechanical impedance. Considering the piezoelectric qualities of the PZT patch, it investigates the relationship between the electrical and mechanical reactions. To simulate concrete-PZT patch interactions, the electrical and solid mechanics domains are coupled. In COMSOL Multiphysics environment, the piezoelectric constitutive equations control the electro-mechanical coupling, simulates wave excitations and sensing. In order to represent how wave, move through solid structures, solid mechanics is guided by wave motion equations. The Appendix A and B shows verification of the numerical results of EMI-based and WP-based methods respectively for embedded PZT configurations (direct) with the corresponding experimental ones, as extracted in literature [20,23]. The reported experimental findings for

direct embedded PZT patch configurations showed acceptable sensitivities in conductance signatures for EMI method (excitation frequency range between 10 and 510 kHz) and P-wave velocities for WP method (time range 20–40 μs), in order to judge the variations of concrete strength development. For design and parametric study of RSB configurations, investigations are then carried out by material model updating for every configuration and model under consideration. More details related to modelling the materials and coupling for various SHM techniques are briefly discussed in the forthcoming subsections.

3.1. EMI technique

In the present study, an indirect attachment through a bolt having epoxy attached squared PZT patch on its head is studied in detail for application of health monitoring of concrete strength. Table 3 depicts different bolt configurations used in the numerical analysis. The RSB-based EMI technique is modelled in the same way as the embedded PZT based EMI technique, the only difference is taking one more material *i.e.*, steel bolt having mass density of 7850 kg/m^3, Poison's ratio of 0.28 and infinite relative permittivity. For optimizing the design of RSBs, three different models of bolts namely Prototype-I (*or say*, P-I) bolt having hexagonal head, Prototype-II (*or say*, P-II) bolt having hexagonal head with disk washer and Prototype-III (*or say*, P-III) bolt with squared head of standard specifications as specified by Indian standard organization are considered. The main purpose of considering three different bolts configurations (*i.e.*, P-I, P-II and P-III) is to get an idea about which
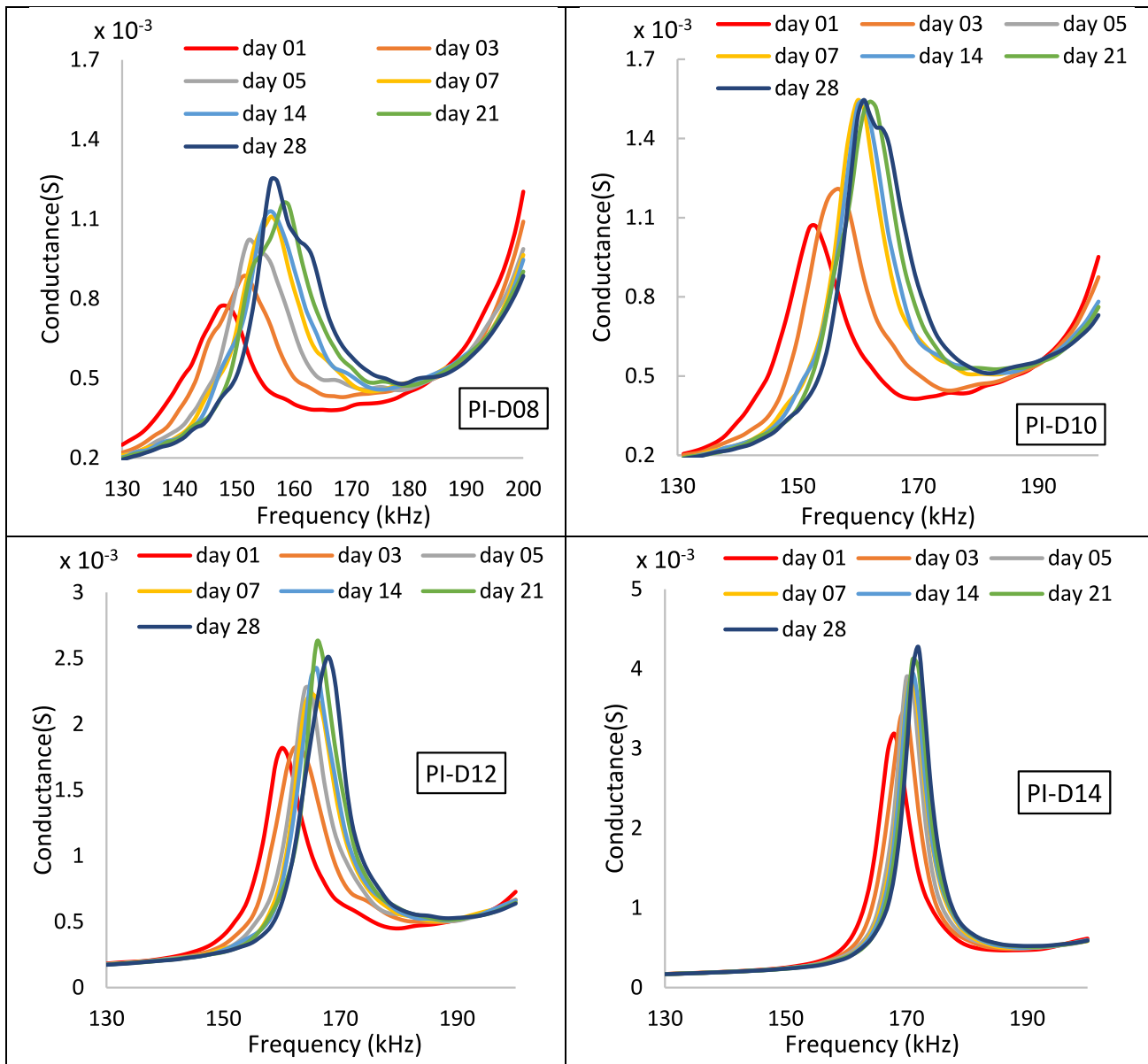
Fig. 9. Conductance signatures obtained at different concrete age upon altering bolt shank diameter from 08 to 14 mm for Prototype-I.

bolt type and PZT patch location on bolt yields higher EMI output sensitivity for effective monitoring of concrete strength development.

Further, the bolt shank length (for Prototype-I, II and III), bolt shank diameter (for Prototype-I and III), bolt head thickness (for Prototype-I and III), washer thickness & washer external diameter (for Prototype-II) are varied in order to optimise the dimensions of RSB sensors. Table 4 illustrates the nomenclature of 31 different RSB prototypes based on varying dimensional details used in FE study.

For developing RSB sensors, the PZT patch was attached to bolt head in PI and PIII, whereas it is attached to washer in PII, considering the epoxy layer between PZT patch and bolt head surface in all the cases. To access the concrete health, the shank region was inserted in the concrete cube model of size $150 \times 150 \times 150$ mm^3 for completely transfer of the strain induced through the PZT patch to the substrate. Fig. 2 represents meshed models of free and combined RSB's Prototypes-I, II and III with concrete cubes. The meshing statistics and sizes considered for all models developed are illustrated in Tables 5 and 6 respectively.

3.2. WP technique

To demonstrate the wave propagation simulation using RSBs, a 3D concrete cube model of $150 \times 150 \times 150$ mm^3 in size having two RSBs with bolt's shank inserted in the concrete at opposite faces is considered as shown in Fig. 3(a). Fig. 3(b) illustrates the meshed finite element model of cubes with two RSBs. The RSBs are attached to opposite face of cube, one being enacting as actuator and the other as sensors. The sort of finite element mesh used in this study is free tetrahedral, and it is a second-order polynomial interpolation function element. The FE meshes of the RSBs, adhesive layers, and concrete cube be separated in order to simulate waves. The mesh size for the concrete cube is affected by wavelengths of the P- and S- waves. The phase velocities of the S_0 mode and A_0 mode for the wave at 100 kHz on the concrete cube with a width of 150 mm are taken as 3600 m/s and 2000 m/s, respectively. As a result, the concrete cube's highest mesh size and smallest mesh size are set to 3600/f_0/1.5 mm and 1.0 mm, respectively. Similar to this, the PZT's mesh size is set to 3900/f_0/5.0 mm. The entire meshes consist of around 5935 tetrahedral components, 936 triangle elements and 132 edge elements. One simulation takes about 8 h to render in actual
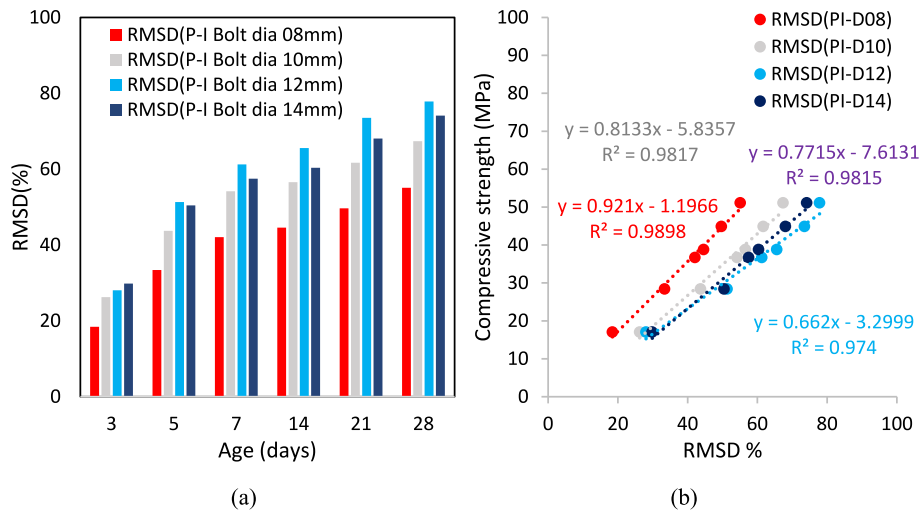
Fig. 10. (a) RMSD index of *G* for model PI on varying bolt shank diameter and concrete age, and (b) Corresponding correlation between strength and RMSD for PI model.

calculation time.

4. Results and discussion

With change in properties of concrete for increasing curing days, the variation in real part of impedance *i.e.,* conductance and P-wave velocities are obtained numerically. The conductance signatures and P-wave velocities are firstly compared with the experimental results from literature for embedded configurations of PZT patch while implying EMI and WP techniques. Then, different RSB configurations are explored for improvised compressive strength development monitoring of concrete cubes.

For all model and configurations, the RMSD index is plotted taking conductance signature of day-01 concrete age as baseline. The reason behind using day-01 signatures as baseline, instead of day-0, is that concrete surface is moist and didn't achieve much stiffness resulting inconsistent non-repeatable outputs during very-early hydration ages. At present, for monitoring early-age concrete strength development, these RMSD indices values are evaluated and linearly correlated with the gain in concrete's compressive-strength relative to curing duration from day 01 to day 28. Furthermore, the Relative time of flight (RTOF) for WP, and RRF for EMI technique are determined for all RSB configuration. These RTOF and RRF values are then matched with the compressive-strength of concrete cube to give better correlation for proving RSB efficacy in monitoring strength development of concrete during hydration.

4.1. Strength monitoring using EMI technique

The EMI responses of all free-RSB sensors (Prototypes -I, -II and -III) are firstly obtained numerically before utilising it for concrete strength monitoring. In case of free-RSBs (*i.e.,* RSB not connected to concrete cube), the PZT patch is glued to bolt heads of various considered steel bolts as mentioned in Section 3. The PZT patch is then polarised electrically and actuated in the frequency range of 10–510 kHz at 200 Hz interim period to get the *G* & *B* responses as depicted in Fig. 4. Multiple resonant frequency peaks are obtained mainly in PZT excitation frequencies between 100 and 600 kHz for all free-RSB prototypes (PI, PII, and PIII).

The shank portion of RSBs is then inserted inside the mid-surface of concrete cube to get the combined EMI response. The conductance being more sensitive [19,63] is considered for sensing outputs upon varying concrete age and bolts geometry. It can be found from literature that in case of concrete substrates, 100–500 kHz frequency ranges show higher

sensitivity of EMI response. A shorter excitation frequency range was selected to excite PZT patch in order to decrease analysis time. Fig. 5 shows variations in the conductance signatures (in PZT excitation frequency ranges between 130 and 200 kHz) of model P-I bolt inserted in concrete cube obtained at curing age between day-01 to day-28 with change in bolt's head thickness from 3.4 to 6.4 mm. For all the models, upon increasing curing age of concrete, the conductance peaks shifted to right-upward direction. The resonant frequency as well conductance peak magnitude increases with concrete age. Also, the peaks observed for 3.4 mm head thickness are seen to be more damped than the peak obtained for 6.4 mm thickness. The magnitude of the conductance peaks increases with thickness of the bolt's head. The corresponding RMSD (in percentage) index obtained relative to concrete age and bolt's head thickness is depicted using bar graph in Fig. 6(a). The rate of change in RMSD observed to be increasing up to 5.4 mm thickness (model PI-H5.4). Fig. 6(b) depicts the linear correlation obtained for RMSD percentage and compressive strength with curing time with good degrees of confident levels.

Variation in the conductance signatures obtained with curing time of day 01 to day 28 taking RSB P-I shank length of 35 mm, 70 mm and 100 mm are plotted in Fig. 7. It can be visualised that with increasing the shank length of the RSB, the smooth trend of signatures distracted, while peaks getting distorted and shifting leftwards. Overall, for all cases, the conductance peaks are observed to be right-upward shifted with concrete age. The corresponding RMSD index for conductance signatures for considered RSB shank length is depicted in Fig. 8(a). The RMSD is observed higher for model PI-L35. On increasing bolt length to 70 mm and 100 mm, RMSD tends to be lower. A shorter bolt length results in less contact between concrete and PZT patch. In the FE simulations, this may lead to a weaker electro-mechanical interaction between the two materials. Due to the decreased coupling, the EMI signatures are more variable, which raises the RMSD values for shorter bolt length. Also, the concentration of stress and strain near bolt and inadequate boundary conditions in FE modelling of shorter length bolt can introduces simulation errors that lead to higher variations in the EMI signatures, resulting in higher RMSD values. Fig. 8(b) represents the linear correlation obtained for RMSD percentage with compressive-strength of concrete.

The distribution of conductance obtained with day 01 to day 28 concrete strength considering RSB P-I shank diameter as 8 mm, 10 mm, 12 mm and 14 mm is plotted in Fig. 9. It can be portrayed that with increasing the shank diameter of the RSB, the peaks are getting pointed and sharper while being shifted in right-upward direction, all observed to localise at the same point near resonant frequency. The corresponding
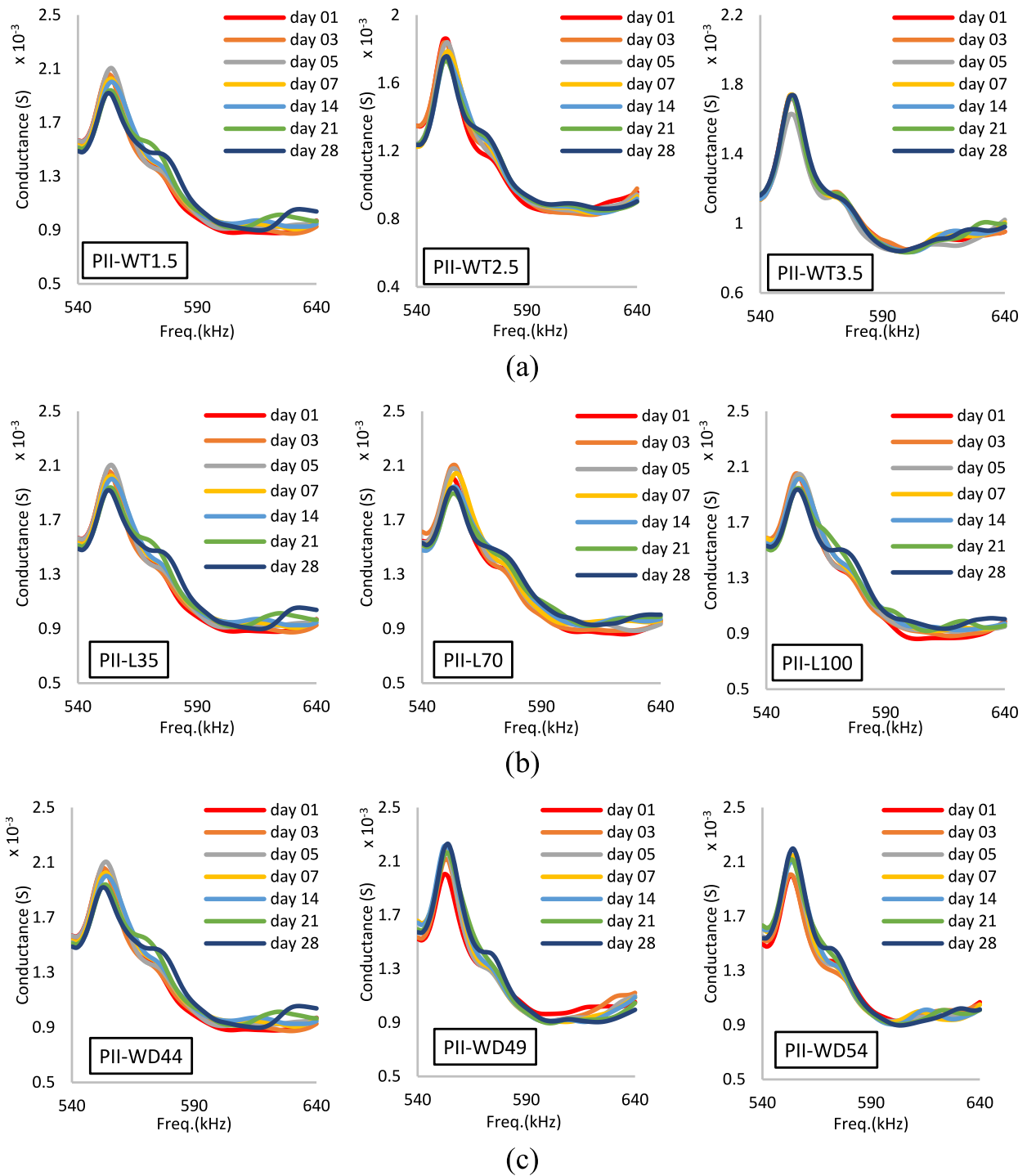
Fig. 11. Conductance signatures obtained at different concrete age for Prototype-II upon altering (a) bolt washer thickness from 1.5 to 3.5 mm, (b) bolt shank length between 35 and 100 mm, and (c) bolt washer external diameter from 44 to 54 mm.

RMSD index for conductance signatures for considered RSB shank diameter is depicted in Fig. 10(a). The RMSD is observed higher for model PI-D12. The linear correlation obtained for RMSD percentage with change in compressive-strength of concrete is represented in Fig. 10(b) with higher confidence levels.

In the similar way, the FE analysis has been carried out to get the impedance distribution with excitation frequency of PZT patch for all the cases of RSB sensors Prototype-II inserted in concrete cube. Fig. 11 (a, b and c) depicts the variations in conductance relative to bolt's washer thickness (1.5 mm, 2.5 mm and 3.5 mm), shank length (35 mm,

70 mm and 100 mm), and washer external diameter (44 mm, 49 mm and 54 mm) respectively. The conductance signature observed shifted left-downward on increasing concrete age. The corresponding RMSD index plotted for all the cases in Fig. 12 (a, b, and c) revealed the maximum deviation observed for washer thickness 1.5 mm, shank length 35 mm, and external washer diameter 49 mm which make suitable for its utilization as RSB sensors for monitoring concrete strength with maximum sensitivity. Fig. 12 also shows the corresponding linear correlation of RMSD with concrete's compressive-strength for RSB P-II prototypes. Overall, the RMSD of P-II types RSB diminished to around 10 times when
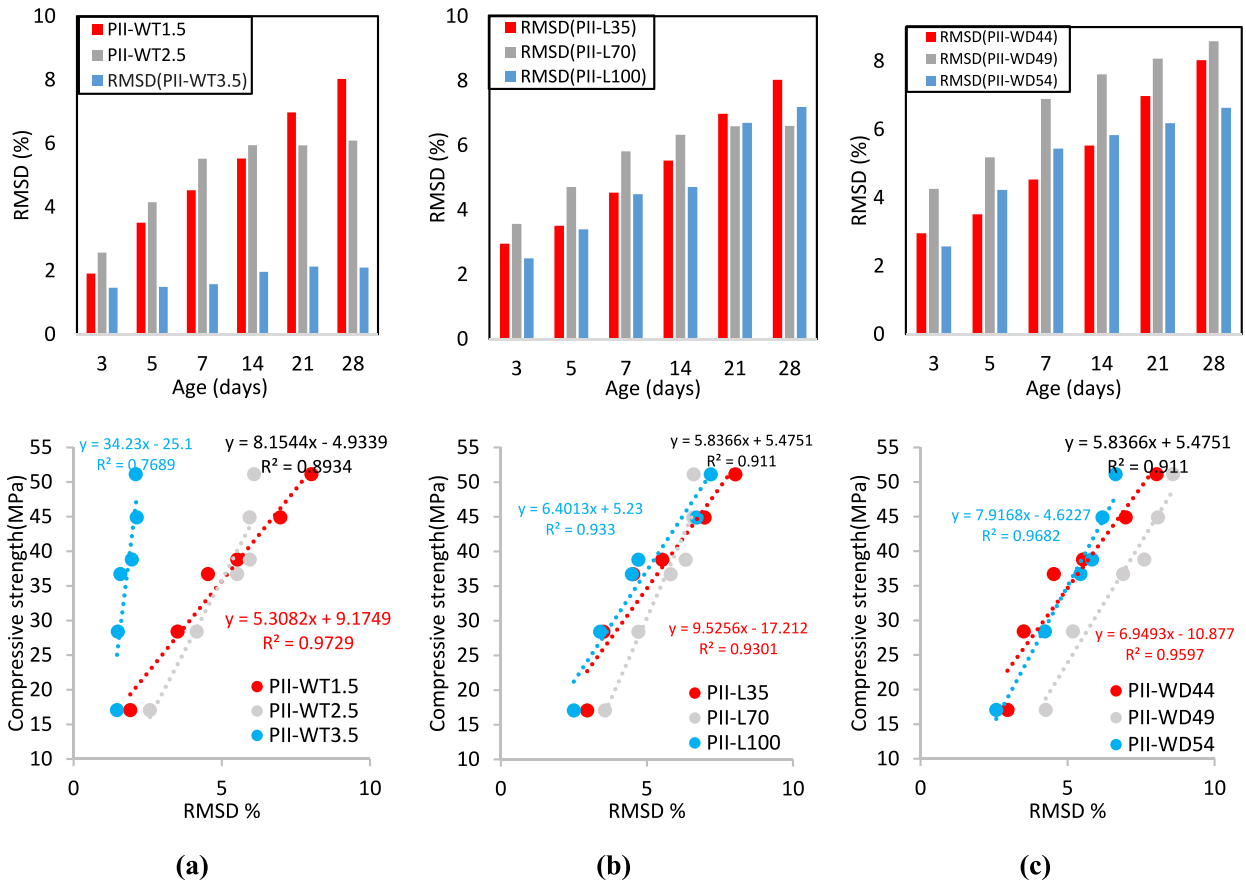
Fig. 12. RMSD index and corresponding correlation between strength and RMSD for PII model upon variation in (a) washer thickness from 1.5 to 3.5 mm, (b) bolt shank length from 35 to 100 mm, and (c) washer external diameter from 44 to 54 mm.

compared that of P-I types. This is due to the reason that PZT patch is not directly attached to bolt, but bonded to the washer, which causes much lower transfer of strains actuated and sensed by transducers.

The conductance spectrum of RSB Prototype-III sensors inserted in concrete cube upon varying bolt's head thickness (3.4 mm, 4.4 mm, 5.4 mm and 6.4 mm), shank length (35 mm, 70 mm and 100 mm), and shank diameter (8 mm, 10 mm, 12 mm and 14 mm) is delineated in Fig. 13. (a, b & c) respectively. The conductance signature seems to be shifted in right-upward direction on increasing concrete age. The corresponding RMSD index plotted for all the cases in Fig. 14 (a, b, & c) revealed the maximum sensitivity is observed for head thickness 6.4 mm, shank length 100 mm, and shank diameter 14 mm. Fig. 14 also shows the corresponding linear correlation of RMSD with concrete's compressive-strength for RSB P-II prototype with good confidence levels. Overall, the sensitivity of P-III types RSBs found comparably lower than P-I type RSBs but around eight time higher than of P-II types RSBs while monitoring concrete strength.

4.2. Strength monitoring using WP technique

In present numerical study, a sinusoidal tone burst-transient voltage at a certain frequency (*i.e.*, the actuation signal) was applied at actuating transducer across its polarisation direction. The actuating smart patch was deformed to induce elastic vibrations by the converse-piezoelectric effect. The actuating frequencies used in this investigation was 60 kHz. A waveform travels radially through the concrete as a result of the actuator's vibratory reaction. Through the direct piezoelectric action, the sensing patch transformed the incoming elastic wave into electrical voltages (*i.e.*, the sensing signal). The tone-burst stimulation may be used to produce a variety of waves, such as P-waves, shear-waves, R-

waves, and other wave modes. The P-wave velocity was used in the ongoing investigation to diagnose the concrete's strength progression during curing process. The P-wave may easily be recognised as the first-wave packet from the sensing signatures since it is often a non-dispersive wave with the fastest rate of propagation. Therefore, the triggering signals have no effect on P-wave velocities. By dividing the center-to-centre distance between the PZT transducers by the wave's travel duration (*i.e.*, TOF), the velocity of a P-wave may be calculated. P-wave velocity can be determined by estimating TOF of corresponding signal peaks for different health states of concrete.

The change in terminal voltage peaks obtained with concrete curing age (day 01 to day 28) for concrete cube modelled with RSBs (PI-H6.4) on opposite faces. The P-I configuration of 6.4 mm bolt thickness was selected for modelling the WP-based method due to the fact that it showed higher sensitivity in EMI-based methods when compared to other RSB's configuration (P-II and P-III models) (refer to Figs. 5–14). It can be visualised from Fig. 15 that as the strength of the concrete specimen increases upon hydration, the time of flight as well as magnitude of the terminal voltage peaks of wave decreases.

The comparison of WP and EMI technique for concrete cube with RSB(PI-H6.4) is done for calibrating the interrelation between the two methodologies. Firstly, for EMI technique, the normalized resonance frequency is determined with respect to highest frequency (known as relative resonance frequency) for models at different curing age (*i.e.*, 1, 3, 5, 7, 14, 21, and 28 days). The exponential relationship is developed between gain in concrete strength and relative resonance frequency, which is found to be better correlated with coefficient of determination (R^2) of 0.9182 as shown in Fig. 16(a). The concrete's compressive strength can also be predicted using Fig. 16(b), plotted to relate normalized RMSD values at different curing days. The normalised RMSD
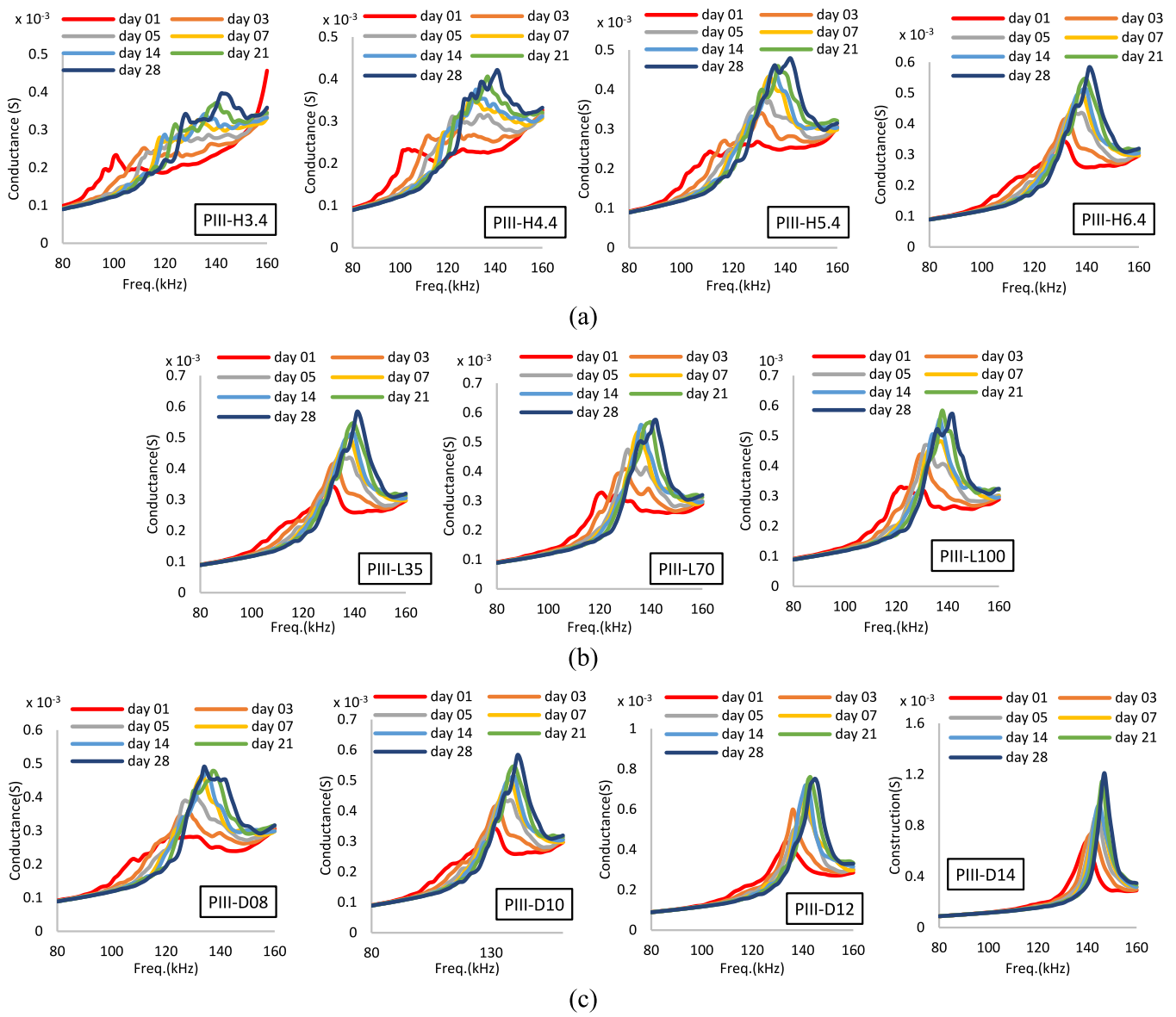
Fig. 13. Conductance signatures obtained at different concrete age for Prototype-III upon altering (a) bolt head thickness between 3.4 and 6.4 mm, (b) bolt shank length between 35 and 100 mm, and (c) bolt shank diameter between 8 and 14 mm.

is defined as the relative RMSD at any curing day with respect to RMSD at 28th curing day. Afterward, RRF shift of EMI technique, & P-wave velocities of WP technique are correlated with coefficient of determination (R^2) of 0.9272 (*see* Fig. 16(c)). However, when compared to Tang's study for concrete beam with embedded transducers, the presently used RSB configuration shows lesser sensitivity in RRF shifting from 1 to 0.906 for P-wave velocities from 3533 m/s to 4274.2 m/s as represented in Fig. 16(c). But on the other side, for WP technique, the change in compressive strength from 6.65 MPa to 51.11 MPa shows significant variations in P-wave velocities from 3533 m/s to 4274.2 m/s respectively which proves the efficacy of methodology in hydration monitoring applications (Fig. 16(d)). For strength calibration, the exponential relationship shown in Eq. (6) is proposed for concrete strength (*f*) relative to P-wave velocity (*v*), which is found to be correlated with coefficient of determination (R^2) of 0.8515.

$$f = 0.0034e^{0.0023v} \ ; \ R^2 = 0.8515 \tag{6}$$

Overall, the shift of P-wave velocity in WP technique and RMSD index for conductance in EMI technique results proficient in capturing

development of concrete strength using RSBs with higher sensitivities. These shifting in output signals of both techniques upon concrete strength variation are correlated in Fig. 16(e). Eq. (7) is proposed with 98.6 % confidence level to correlate the EMI and WP technique results.

$$v_r = 0.9605D^2 - 0.1353D; \ \ R^2 = 0.9866 \tag{7}$$

where, v_r is relative change in P-wave velocities, and *D* is RMSD magnitude for conductance signatures. The paper will lead to development of new non-destructive technique, having RSB sensors of optimal dimensions that can be reused for concrete's structural health monitoring. The proposed study is first of its kind that relates hybrid EMI and WP technique with strength gain of conventional-used concrete using RSB sensors. However, more studies utilising different kind of concrete mixes and input parameters are required to generalised the technique for all concrete mixes.

5. Conclusions

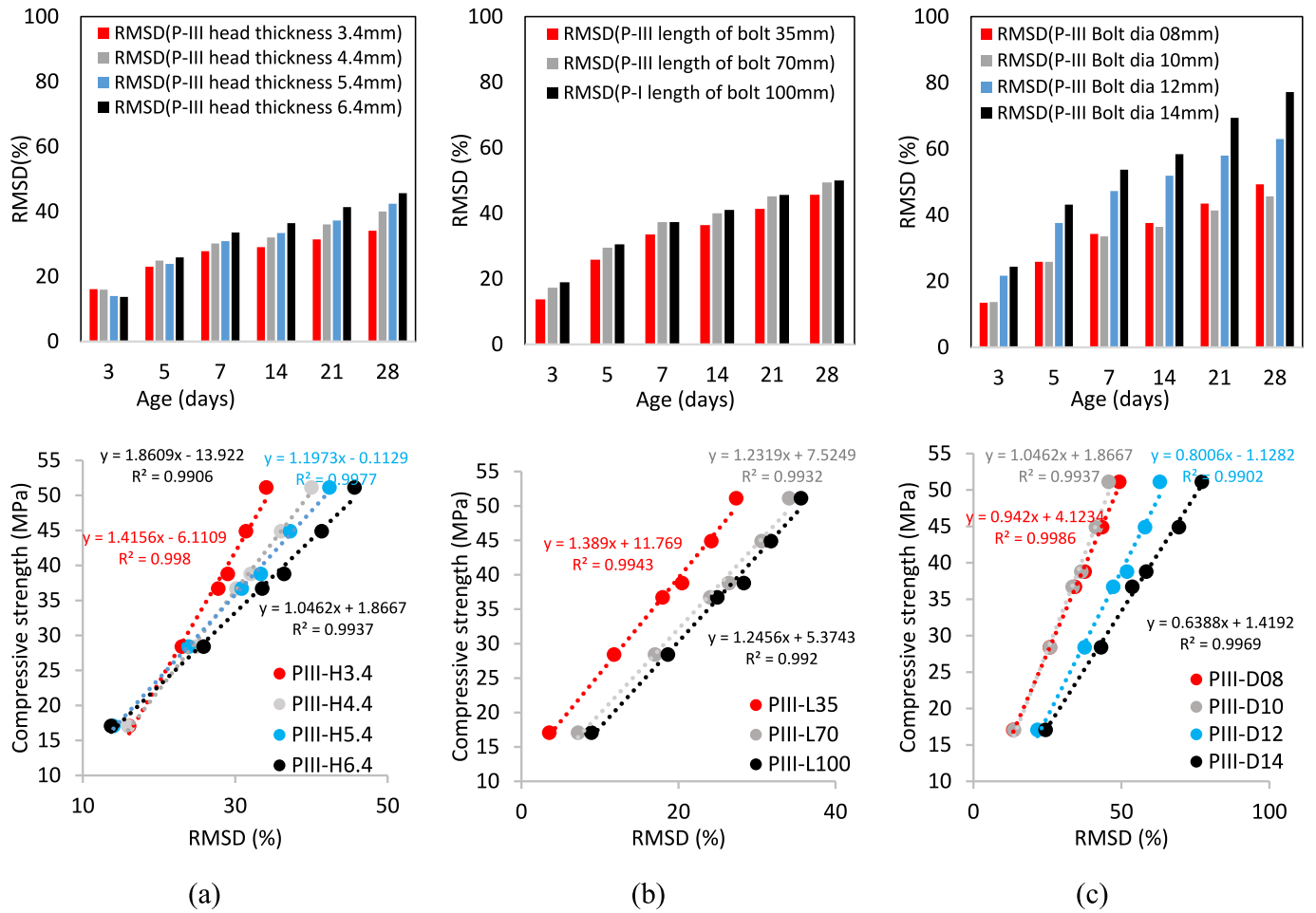The PZT-structure interaction for monitoring concrete strength

Fig. 14. RMSD index and corresponding correlation between strength and RMSD for PIII model upon variation in bolt (a) head thickness from 3.4 to 6.4 mm, (b) shank length from 35 to 100 mm, and (c) shank diameter from 8 to 14 mm.
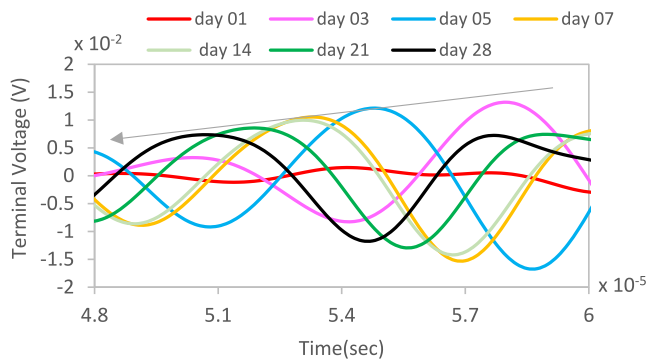

Fig. 15. Variation of terminal voltage (first peak) at receiver RSB with concrete age.

development during hydration has been successfully demonstrated through numerical modelling using hybrid EMI and WP techniques. The peaks of conductance and propagating wave velocities shows better sensitivity upon varying concrete characteristics for all the considered RSB cases. The validation of numerical results with experimental from literature for both techniques is carried out successfully with higher accuracy. Besides conventionally-used surface-bonded and embedded piezo patches, the indirectly-bonded RSB configurations shows tremendously good results of piezo outputs for effective and low-cost application in concrete health monitoring while capturing impedance

signatures in EMI technique, and P-wave velocities in WP technique. The parametric study reveals the optimum design for RSB Prototype P-I having bolt's head thickness-6.4 mm, shank length-35 mm and shank diameter-12 mm. The PZT patch attached to head of square bolts (P-III model) shows less sensitivity of RMSD index when compared to that of PZT patch bonded to head of circular bolts without washer (P-I model). For RSB to be proficient in monitoring, bonding the PZT patch to bolt-head instead to its washer results 10 times better sensitivity in the output signals. Further, proposed mathematical models for RMSD helps the future researcher to judge the shifting of RSB-identified impedance signatures for estimating the concrete strength with higher accuracy. On the other side, the strength calibration charts relative to RSB identified P-wave velocities and RRF are successfully proposed. The concrete strength development shows exponential growth relative to both RRF and P-wave velocities. Overall, the increment in P-wave velocity with strength development of concrete is correlated to RMSD of PZT-identified conductance with higher confidence levels. Future studies may focus on estimating RSB-identified equivalent stiffness parameters (k-m-c) using EMI technique for investigating inherent characteristics of concrete matrix that could be useful for developing for low-cost and prominent health monitoring solutions.

Conflict of Interest Statement.

The authors declare no potential conflicts of interest with respect to the research, authorship, and/or publication of this article.
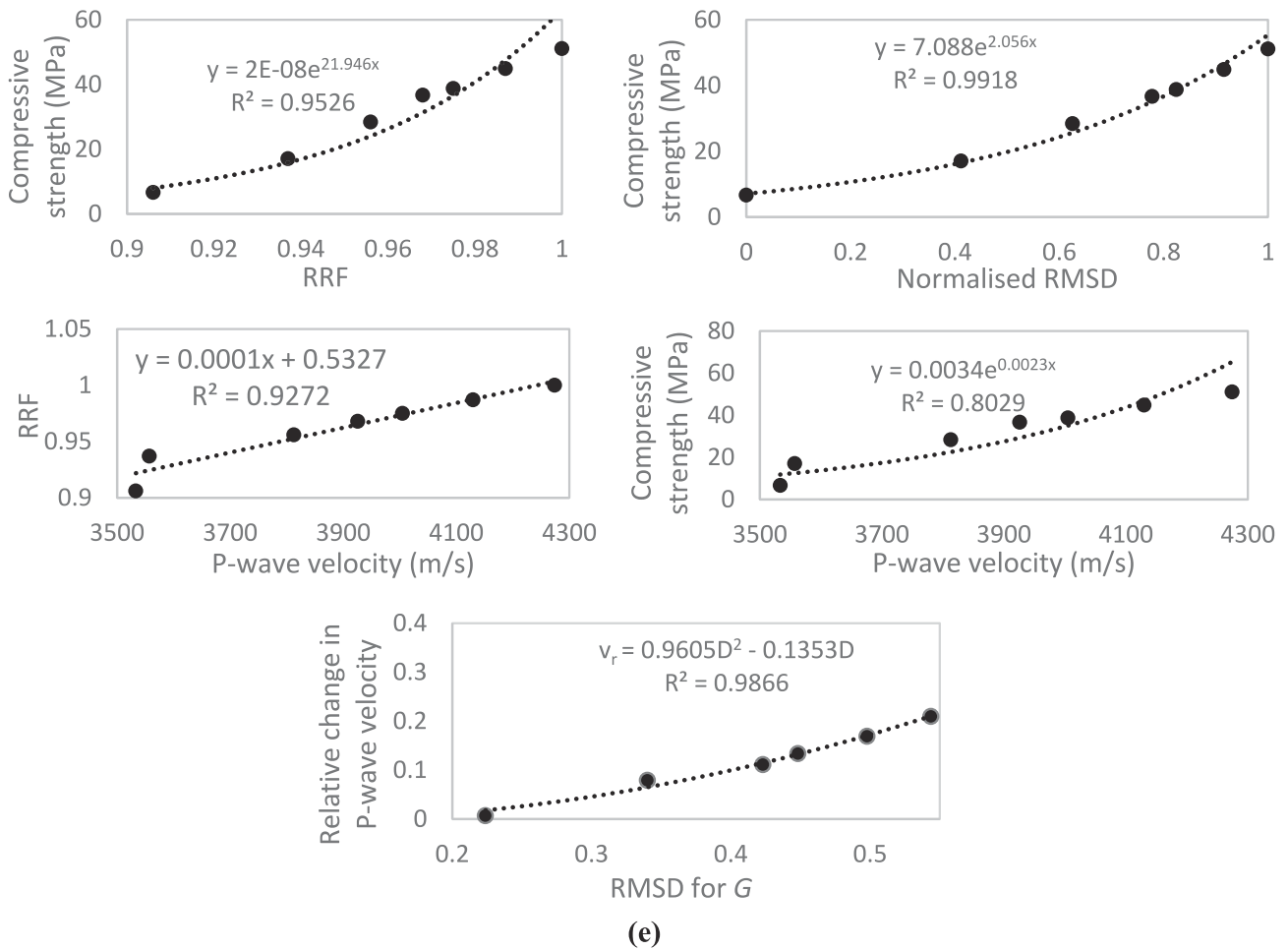
Fig. 16. Strength calibration chart for (a) Compressive strength vs. relative resonance frequency (EMI technique), (b) Compressive strength vs. normalized RMSD (EMI technique), (c) RRF vs. P-wave velocity, (d) Compressive strength vs. P-wave velocity (WP technique), and (e) Relationship between outputs of EMI and WP technique results [~Model: Concrete cube with RSB PI-H6.4 sensor].
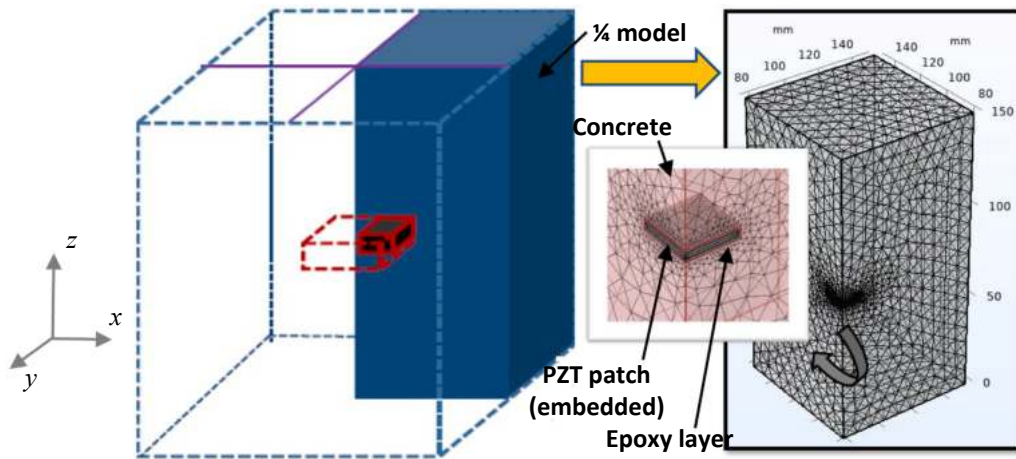

Fig. A1. FE model created for validation of EMI technique (Model: Concrete cube with embedded PZT patch).

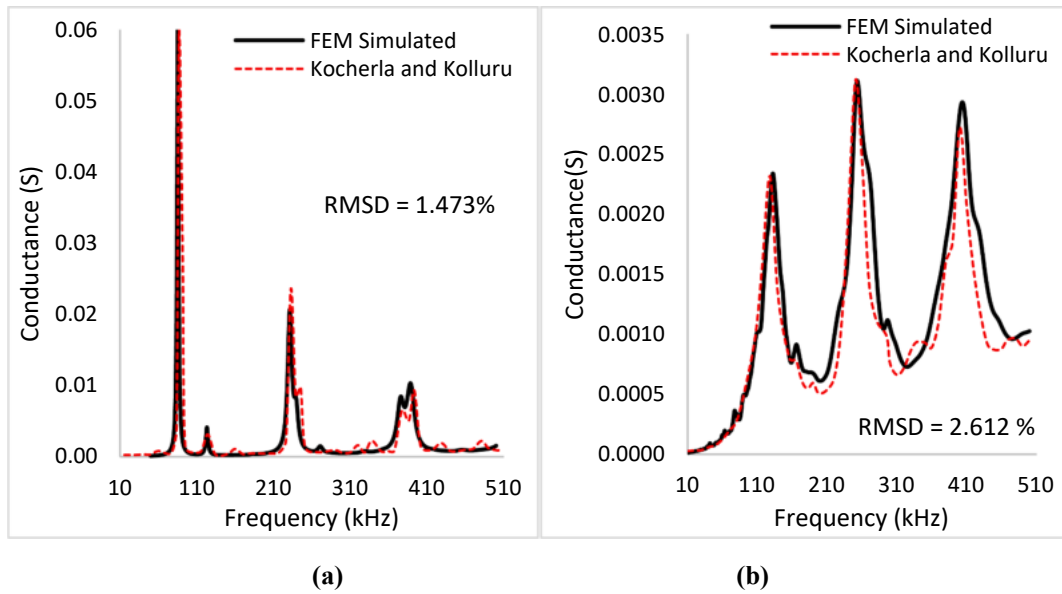## CRediT authorship contribution statement

Fig. A2. Validation of EMI results obtained in present numerical study with experimental obtained by [23], for (a) Free PZT patch, and (b) PZT patch embedded in concrete cube at 28 day age.
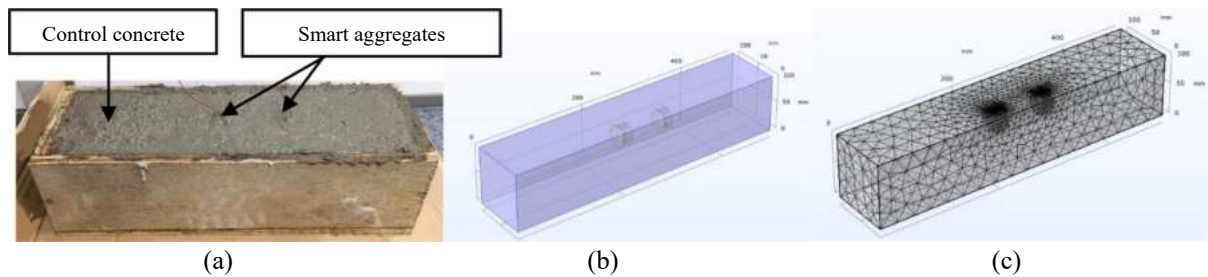

Fig. B1. (a) Concrete control beam considered by Tang et al. (2022) [20], (b) Isometric view of beam modelled with embedded sensors, and (c) Meshed view of model.
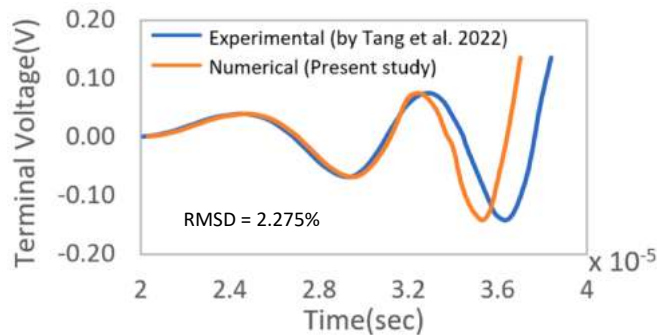

Fig. B2. Validation of numerical results for signal response at receiver transducer.

Declaration of Competing Interest

The authors declare that they have no known competing financial interests or personal relationships that could have appeared to influence the work reported in this paper.

Appendix A. Verification of EMI results

To validate the results of EMI technqiue extracted via numerical modelling, the FE models of concrete cube of size $150 \times 150 \times 150$ mm^3 with embedded PZT patch with epoxy coating inside the concrete matrix are generated as done in experimental study demonstrated by Kocherla and Kolluru [23]. To simulate the experimental study, the comparison of conductance signatures is demonstrated for verifying the FE results. The 3D-numerical model developed in present study is shown in Fig. A1. Quarter model having cross sectional area of $75 \times 75 \times 150$ mm^3 is created using symmetry in FE modelling. Using the symmetry property, the model is analysed by deleting 3/4th domains, as one-fourth remaining give the same results with lesser analysis time using workplane symmetry property of COMSOL Multiphysics. Instead, one simulation takes around 12 h to render in actual calculation time. The condition for using symmetry is that it should be used along *zx* or *zy* plane *i. e.,* polarization axis of the PZT patch along *z*-axis. A epoxy layer of 3 mm thickness is considered all-round the PZT patch surface boundary. The voltage of 1 V is applied perpendicularly to the *x-y* plane *i.e.* towards the polarization axis with excitation frequency sweep in range between 10 and 500 kHz at 408 Hz interim period. The total number of tetrahedron-elements in the comprehensive embedded PZT model are 44435, of which 5268 are triangular and 397 are edge-elements. The smallest element size is 0.6 mm, which was purposefully chosen to be smaller

than epoxy thickness in order to account for the bond layer's participation in the study. The largest element size was considered to be 8.25 mm during FEM.

The free PZT patch response (*i.e.*, without attaching PZT patch with the concrete matrix) obtained numerically is plotted to simulate the experiment demonstrated by Kocherla and Kolluru [23] in the PZT excitation frequency ranges between 10 and 510 kHz as shown in Fig. A2 (a). To validate the EMI response, the similar properties taken by [23] were used as inputs for numerical modelling. The comparison of signatures obtained experimentally by [23] while embedding the PZT patch inside the concrete cube at 28-day age with the signature obtained numerically at present is also represented in the Fig. A2(b). Due to the influence of external factors in experimentations such as the unevenness of the adhesive layer, non-homogeneity of concrete, losses incurred, impedance curve may be seen somewhat deviating from experimental values. But overall, the results validate the EMI response of free and embedded configuration (with epoxy protective layers inside the concrete cube) of PZT patch with the RMSD of 1.473 % and 2.612 % respectively. A close similarity between experimental and numerical values is observed that shows the efficacy of using numerical techniques in extracting EMI spectrum of PZT-structure interaction useful for health monitoring methodologies.

Appendix B. Verification of WP results

For validating the WP technique, the outcomes of numerical modelling are initially compared with experimentally-obtained ones demonstrated by Tang et al. (2022) [20] for monitoring concrete strength. Firstly, a 3D beam model of size $500 \times 100 \times 100$ mm^3 with two embedded smart cylindrical aggregates (containing PZT patch $20 \times 20 \times 5$ mm^3 in 1:6 cement matrix) having 35 mm diameter, 16 mm height each and vertically placed at spacing of 80 mm c/c is developed (*refer to* Fig. B1 (a) and (b)). Other mechanical and electrical properties are considered same as taken for experimentations and can be referred from [20]. At present for FE study, the predefined tetrahedral fine mesh is chosen for simulations. Fig. B1(c) shows the isometric view of meshing geometry of the developed model. The entire meshes consist of around 16,894 tetrahedral components, 3546 triangle elements and 329 edge elements. The maximum element size is 40 mm and the curvature factor is 0.5 mm.

Fig. B2 shows the comparison of experimentally and numerically obtained signal received at sensor transducer for direct-embedded configurations. The dissimilarity of peaks for higher wave levels may be due to considering concrete material to be homogeneous and isotropic in numerical modelling. The RMSD of 2.275 % for TOF of first signal peak was observed between numerical & experimental results. Therefore, due to close similarity, the shifting of first peak of received signal is taken into consideration for estimating change of P-wave velocities at different health states.

References

[1] Isah BW, Mohamad H, Ahmad NR. Rock stiffness measurements fibre Bragg grating sensor (FBGs) and the effect of cyanoacrylate and epoxy resin as adhesive materials. Ain Shams Eng J 2021;12:1677–91. https://doi.org/10.1016/j.asej.2020.09.007.

[2] Morshed AHE, Atta RM. Multimode optical fiber strain monitoring for smart infrastructures. Ain Shams Eng J 2023:102181. https://doi.org/10.1016/j.asej.2023.102181.

[3] Haq M, Bhalla S, Naqvi T. Piezo-impedance based fatigue damage monitoring of restrengthened concrete frames. Compos Struct 2022;280. https://doi.org/10.1016/j.compstruct.2021.114868.

[4] Ji Y, Chen A, Chen Y, Han X, Li B, Gao Y, et al. A state-of-the-art review of concrete strength detection/monitoring methods: with special emphasis on PZT transducers. Constr Build Mater 2023;362. https://doi.org/10.1016/j.conbuildmat.2022.129742.

[5] Clemente CS, Davino D, Loschiavo VP. Magnetostrictive materials and energy harvesting for structural health monitoring applications. IOP Conf Ser Mater Sci Eng 2020;949. https://doi.org/10.1088/1757-899X/949/1/012012.

[6] Ghosh DP, Gopalakrishnan S. Structural health monitoring in a composite beam using magnetostrictive material through a new FE formulation. Smart Mater Struct Syst 2003;5062:704. https://doi.org/10.1117/12.514687.

[7] Song G, Mo YL, Otero K, Gu H. Health monitoring and rehabilitation of a concrete structure using intelligent materials. Smart Mater Struct 2006;15:309–14. https://doi.org/10.1088/0964-1726/15/2/010.

[8] Davis AM, Mirsayar MM, Hartl DJ. A novel structural health monitoring approach in concrete structures using embedded magnetic shape memory alloy components. Constr Build Mater 2021;311. https://doi.org/10.1016/j.conbuildmat.2021.125212.

[9] Aggelis DG, Mpalaskas AC, Matikas TE, Van Hemelrijck D. Acoustic emission signatures of damage modes in structural materials. Nondestruct Charact Compos Mater Aerosp Eng Civ Infrastruct, Homel Secur 2013;2013(8694):86940T. https://doi.org/10.1117/12.2008942.

[10] Mpalaskas AC, Matikas TE, Aggelis DG. Acoustic monitoring for the evaluation of concrete structures and materials. Acoust Emiss Relat Non-Destructive Eval Tech Fract Mech Concr Fundam Appl 2020:257–80. https://doi.org/10.1016/B978-0-12-822136-5.00013-7.

[11] Roopa A, Hunashyal AM. Evaluating self-sensing property of carbon fibre cement composite by experimental study and finite element modelling for structural health monitoring applications. IOP Conf Ser Mater Sci Eng 2021;1070:012041. https://doi.org/10.1088/1757-899x/1070/1/012041.

[12] Boehle M, Jiang Q, Li L, Lagounov A, Lafdi K. Carbon nanotubes grown on glass fiber as a strain sensor for real time structural health monitoring. Int J Smart Nano Mater 2012;3:162–8. https://doi.org/10.1080/19475411.2011.651509.

[13] Ahamed R, Choi SB, Ferdaus MM. A state of art on magneto-rheological materials and their potential applications. J Intell Mater Syst Struct 2018;29:2051–95. https://doi.org/10.1177/1045389X18754350.

[14] Lessly SH, Rajendran S. Measurement of core bond strength in reinforced concrete column using magneto rheological fluid assisted Ultrasonic measuring technique. Nondestruct Test Eval 2022;37:134–59. https://doi.org/10.1080/10589759.2021.1939697.

[15] Crawley EF, De Luis J. Use of piezoelectric actuators as elements of intelligent structures. AIAA J 1987;25:1373–85.

[16] Liang C, Sun FP, Rogers CA. An impedance method for dynamic analysis of active material systems; 1994. http://asme.org/terms.

[17] Bhalla S, Soh CK. Structural health monitoring by piezo-impedance transducers. I: modeling, J Aerosp Eng 2004;17:154–65. doi: 10.1061/(asce)0893-1321(2004)17:4(154).

[18] Rosyidi SAP, Yusoff NIM, Ismail NN, Yazid MRM. Integrated time-frequency wavelet analysis and impulse response filtering on SASW test for rigid pavement stiffness prediction. Ain Shams Eng J 2021;12:367–80. https://doi.org/10.1016/j.asej.2020.05.006.

[19] Haq M, Bhalla S, Naqvi T. Fatigue damage and residual fatigue life assessment in reinforced concrete frames using PZT-impedance transducers. Cem Concr Compos 2020;114. https://doi.org/10.1016/j.cemconcomp.2020.103771.

[20] Tang ZS, Lim YY, Smith ST, Mostafa A, Lam AC, Soh CK. Monitoring the curing process of in-situ concrete with piezoelectric-based techniques – a practical application. Struct Heal Monit 2023;22:518–39. https://doi.org/10.1177/14759217221087916.

[21] Karayannis CG, Golias E, Naoum MC, Chalioris CE. Efficacy and damage diagnosis of reinforced concrete columns and joints strengthened with FRP ropes using piezoelectric transducers. Sensors 2022;22. https://doi.org/10.3390/s22218294.

[22] Voutetaki ME, Naoum MC, Papadopoulos NA, Chalioris CE. Cracking diagnosis in fiber-reinforced concrete with synthetic fibers using piezoelectric transducers. Fibers 2022;10. https://doi.org/10.3390/fib10010005.

[23] Kocherla A, Subramaniam KVL. Embedded smart PZT-based sensor for internal damage detection in concrete under applied compression. Measurement 2020;163: 108018. https://doi.org/10.1016/j.measurement.2020.108018.

[24] Liang C, Sun FP, Rogers CA. Coupled electromechanical analysis of piezoelectric ceramic actuator-driven systems: determination of the actuator power consumption and system energy transfer. In: Smart Struct Mater 1993 Smart Struct Intell Syst. SPIE; 1993. p. 286–98.

[25] Zhou S-W, Liang C, Associates R, Asme M, Rogers CA. An impedance-based system modeling approach for induced strain actuator-driven structures; 1996. http://vibrationacoustics.asmedigitalcollection.asme.org/.

[26] Bhalla S, Soh CK. Structural health monitoring by piezo–impedance transducers. II: applications. J Aerosp Eng 2004;17:166–75. doi: 10.1061/(asce)0893-1321(2004)17:4(166).

[27] Wang D, Song H, Zhu H. Embedded 3D electromechanical impedance model for strength monitoring of concrete using a PZT transducer. Smart Mater Struct 2014; 23. https://doi.org/10.1088/0964-1726/23/11/115019.

[28] Tawie R, Lee H-K. Characterization of cement-based materials using a reusable piezoelectric impedance-based sensor. Smart Mater Struct 2011;20:85023.

[29] Yang Y, Divsholi BS, Soh CK. A reusable PZT transducer for monitoring initial hydration and structural health of concrete. Sensors 2010;10:5193–208. https://doi.org/10.3390/s100505193.

[30] Raju J, Bhalla S, Visalakshi T. Pipeline corrosion assessment using piezo-sensors in reusable non-bonded configuration. NDT E Int 2020;111:102220.

[31] Moharana S, Bhalla S. Development and evaluation of an external reusable piezo-based concrete hydration-monitoring sensor. J Intell Mater Syst Struct 2019;30: 2770–88.

[32] Qureshi AR, Shin S-W, Yun C-B. Monitoring of strength gain in concrete using smart PZT transducers. J Korean Soc Nondestruct Test 2007;27(6):501–8.

[33] Shin SW, Oh TK. Application of electro-mechanical impedance sensing technique for online monitoring of strength development in concrete using smart PZT

patches. Constr Build Mater 2009;23:1185–8. https://doi.org/10.1016/j.conbuildmat.2008.02.017.

[34] Lee CJ, Lee JC, Shin SW, Kim WJ. Investigation of setting process of cementitious materials using electromechanical impedance of embedded piezoelectric patch. J Korea Inst Build Constr 2012;12:607–14. https://doi.org/10.5345/JKIBC.2012.12.6.607.

[35] Talakokula V, Bhalla S, Gupta A. Monitoring early hydration of reinforced concrete structures using structural parameters identified by piezo sensors via electromechanical impedance technique. Mech Syst Signal Process 2018;99:129–41. https://doi.org/10.1016/j.ymssp.2017.05.042.

[36] Wang D, Zhu H. Monitoring of the strength gain of concrete using embedded PZT impedance transducer. Constr Build Mater 2011;25:3703–8. https://doi.org/10.1016/j.conbuildmat.2011.04.020.

[37] Guo Z, Sun Z. Piezoelectric impedance based elastic modulus monitoring for concrete during curing. Appl Mech Mater 2012;969–73. doi: 10.4028/www.scientific.net/AMM.166-169.969.

[38] Sujie Z, Jeon JY, Jung H-K, Park G, Won C. Experimental investigation of concrete curing and strength estimation using piezoelectric admittance measurements; 2018. http://www.ndt.net/?id=23435.

[39] Lim YY, Smith ST, Soh CK. Wave propagation based monitoring of concrete curing using piezoelectric materials: review and path forward. NDT E Int 2018;99:50–63. https://doi.org/10.1016/j.ndteint.2018.06.002.

[40] Kong Q, Hou S, Ji Q, Mo YL, Song G. Very early age concrete hydration characterization monitoring using piezoceramic based smart aggregates. Smart Mater Struct 2013;22. https://doi.org/10.1088/0964-1726/22/8/085025.

[41] Lim YY, Majain N, Kwong KZ, Liew WYH. On the study of concrete hydration process using piezoelectric based surface wave propagation technique. ACMSM 2014;23:1121–8.

[42] Lim YY, Kwong KZ, Liew WYH, Soh CK. Practical issues related to the application of piezoelectric based wave propagation technique in monitoring of concrete curing. Constr Build Mater 2017;152:506–19.

[43] Su YF, Han G, Amran A, Nantung T, Lu N. Instantaneous monitoring the early age properties of cementitious materials using PZT-based electromechanical impedance (EMI) technique. Constr Build Mater 2019;225:340–7. https://doi.org/10.1016/j.conbuildmat.2019.07.164.

[44] Feng Q, Liang Y, Song G. Real-time monitoring of early-age concrete strength using piezoceramic-based smart aggregates. J Aerosp Eng 2019;32:04018115. https://doi.org/10.1061/(asce)as.1943-5525.0000939.

[45] Zhang C, Panda GP, Yan Q, Zhang W, Vipulanandan C, Song G. Monitoring early-age hydration and setting of Portland cement paste by piezoelectric transducers via electromechanical impedance method. Constr Build Mater 2020;258. https://doi.org/10.1016/j.conbuildmat.2020.120348.

[46] Luo X, Annamdas VGM, Kiong A, Chee SOH. Strength monitoring of engineered cementitious composites using piezoelectric based smart material. Int Conf Energy Environ Mater 2014.

[47] Ai D, Lin C, Zhu H. Embedded piezoelectric transducers based early-age hydration monitoring of cement concrete added with accelerator/retarder admixtures. J Intell Mater Syst Struct 2021;32:847–66. https://doi.org/10.1177/1045389X20969916.

[48] Lu X, Lim YY, Soh CK. A novel electromechanical impedance–based model for strength development monitoring of cementitious materials. Struct Heal Monit 2018;17:902–18. https://doi.org/10.1177/1475921717725028.

[49] Lu X, Lim YY, Izadgoshasb I, Soh CK. Strength development monitoring and dynamic modulus assessment of cementitious materials using EMI-Miniature Prism based technique. Struct Heal Monit 2020;19:373–89. https://doi.org/10.1177/1475921719848087.

[50] Lim YY, Soh CK. Electro-Mechanical Impedance (EMI)-based incipient crack monitoring and critical crack identification of beam structures. Res Nondestruct Eval 2014;25:82–98. https://doi.org/10.1080/09349847.2013.848311.

[51] Liu W, Giurgiutiu V. Finite element simulation of piezoelectric wafer active sensors for structural health monitoring with coupled-filed elements. In: Sensors Smart Struct Technol Civil, Mech Aerosp Syst 2007. SPIE; 2007. p. 65293R. doi: 10.1117/12.715238.

[52] Yang J, Lim YY, Soh CK. Practical issues related to the application of the electromechanical impedance technique in the structural health monitoring of civil structures: I. Experiment. Smart Mater Struct 2008;17. https://doi.org/10.1088/0964-1726/17/3/035008.

[53] Lu X, Lim YY, Soh CK. Investigating the performance of "Smart Probe" based indirect EMI technique for strength development monitoring of cementitious materials – modelling and parametric study. Constr Build Mater 2018;172:134–52. https://doi.org/10.1016/j.conbuildmat.2018.03.222.

[54] Khan A, Haq M, Naqvi T. Monitoring hydration of concrete using EMI of surface bonded smart piezo patches. Mater Today Proc 2023;80 p.1254-1260. https://doi.org/10.1016/j.matpr.2022.12.270.

[55] Haq M, Naqvi T, Bhalla S, Randhawa J. Numerical assessment of fatigue life of concrete frame using PZT sensors. Sensors Smart Struct Technol Civ Mech Aerosp Syst Proc SPIE 2019;10970:78. https://doi.org/10.1117/12.2513885.

[56] Lalande F, Zaffir C, Rogers CA. Impedance-based modeling of actuators bonded to shell structures. J Intell Mater Syst Struct 1995;6(6):765–75.

[57] Zhou, SW, Liang C, Rogers CA. An impedance-based system modeling approach for induced strain actuator-driven structures; 1996. p. 323–31.

[58] Fairweather, Arthur J. Designing with active materials: an impedance based approach; 1998.

[59] Park S, Ahmad S, Yun C-B, Roh Y. Multiple crack detection of concrete structures using impedance-based structural health monitoring techniques. Exp Mech 2006;46:609–18. https://doi.org/10.1007/s11340-006-8734-0.

[60] Bhalla S, Soh CK. Electromechanical impedance modeling for adhesively bonded piezo-transducers. J Intell Mater Syst Struct 2004;15(12):955–72.

[61] Sumedha M, Bhalla S. Numerical investigations of shear lag effect on PZT-structure interaction: review and application. Curr Sci 2012;103(6):685–96.

[62] Xu YG, Liu GR. A modified electro-mechanical impedance model of piezoelectric actuator-sensors for debonding detection of composite structures. J Intell Mater Syst Struct 2002;13:389–96. https://doi.org/10.1177/104538902761696733.

[63] Negi P, Chakraborty T, Kaur N, Bhalla S. Investigations on effectiveness of embedded PZT patches at varying orientations for monitoring concrete hydration using EMI technique. Constr Build Mater 2018;169:489–98. https://doi.org/10.1016/j.conbuildmat.2018.03.006.

[64] Mhmoud Alzubi K, Salah Alaloul W, Malkawi AB, Al Salaheen M, Hannan Qureshi A, Ali Musarat M. Automated monitoring technologies and construction productivity enhancement: Building projects case. Ain Shams Eng J 2022:102042. https://doi.org/10.1016/j.asej.2022.102042.

[65] Liang C, Sun F, Rogers CA. Electro-mechanical impedance modeling of active material systems. Smart Mater Struct 1996. https://doi.org/10.1088/0964-1726/5/2/006.

[66] Haq M. Application of piezo transducers in biomedical science for health monitoring and energy harvesting problems. Mater Res Express 2019;6(2). https://doi.org/10.1088/2053-1591/aaefb8. p. 022002(1-16).

[67] Kaur N, Bhalla S, Maddu SCG. Damage and retrofitting monitoring in reinforced concrete structures along with long-term strength and fatigue monitoring using embedded Lead Zirconate Titanate patches. J Intell Mater Syst Struct 2019. https://doi.org/10.1177/1045389X18803458.

[68] Bhalla S, Soh CK. Structural health monitoring by piezo-impedance transducers. J Aerosp Eng 2003;17:1–49. https://doi.org/10.1061/(ASCE)0893-1321(2004)17.

[69] Giurgiutiu V, Bao J, Zhao W. Active sensor wave propagation health monitoring of beam and plate structures. In: Smart Struct Mater 2001 Smart Struct Integr Syst. SPIE; 2001. p. 234–45.

[70] Lu Y, Li J, Ye L, Wang D. Guided waves for damage detection in rebar-reinforced concrete beams. Constr Build Mater 2013;47:370–8.

[71] Gu H, Song G, Dhonde H, Mo YL, Yan S. Concrete early-age strength monitoring using embedded piezoelectric transducers. Smart Mater Struct 2006;15:1837–45. https://doi.org/10.1088/0964-1726/15/6/038.

[72] Lim YY, Kwong KZ, Liew WYH, Soh CK. Non-destructive concrete strength evaluation using smart piezoelectric transducer-a comparative study. Smart Mater Struct 2016;25. https://doi.org/10.1088/0964-1726/25/8/085021.

[73] Poorarbabi A, Ghasemi M, Azhdary Moghaddam M. Concrete compressive strength prediction using non-destructive tests through response surface methodology. Ain Shams Eng J 2020;11:939–49. https://doi.org/10.1016/j.asej.2020.02.009.

[74] Song F, Huang GL, Kim JH, Haran S. On the study of surface wave propagation in concrete structures using a piezoelectric actuator/sensor system. Smart Mater Struct 2008;17:55024.

[75] Qin L, Li Z. Monitoring of cement hydration using embedded piezoelectric transducers. Smart Mater Struct 2008;17:55005.

[76] Wahab A, Aziz MMA, MohdSam AR, You KY. Application of microwave waveguide techniques for investigating the effect of concrete dielectric and reflection properties during curing. J Build Eng 2021;38:102209.

[77] Jurowski K, Grzeszczyk S. The influence of concrete composition on Young's modulus. Proc Eng 2015;108:584–91. https://doi.org/10.1016/j.proeng.2015.06.181.

[78] Arif M, Gupta V, Choudhary H, Kumar S, Basu P. Performance evaluation of cement concrete containing sandstone slurry. Constr Build Mater 2018;184:432–9.

[79] Anson M, Newman K. The effect of mix proportions and method of testing on Poisson's ratio for mortars and concretes. Mag Concr Res 1966;18:115–30.

[80] Beushausen H, Dittmer T. The influence of aggregate type on the strength and elastic modulus of high strength concrete. Constr Build Mater 2015;74:132–9.

[81] Haq M, Naqvi T. Numerical assessment of induced damages of RC frames using PZT patch in embedded configurations with and without bond layer. In: Mater Today Proc. Elsevier Ltd; 2020. p. 1977–82. doi: 10.1016/j.matpr.2020.11.430.

[82] Moharana S. Modelling of piezo-structure elastodynamic interaction through bond layer for electro-mechanical impedance technique; 2012.

Dr. Moinul Haq is currently working as Assistant Professor in Department of Civil Engineering, AMU, India since last 4 years. He has obtained his Ph.D and M.Tech degrees in Civil Engineering (Structural Engineering) from the department having research project in collaboration with IIT Delhi. He is an awardee of prestigious direct-SRF National Award by Council of Scientific and Industrial Research (CSIR), India and has qualified GATE exam multiple times. Recently, he is awarded with Best Paper Award 2022 for a research paper presentation titled Monitoring hydration of concrete using EMI of surface bonded smart piezo patches in an international conference held at Mangalore, Karnataka. Dr. Moin does research in areas of Civil and structural engineering, Concrete technology, Structural health monitoring, Piezoelectric sensors and actuators, Bio- and applied-mechanics. He has published around 30 scientific research articles in international journals & conferences and has patented two of his research works by Australian and Indian Patent Office. He has presented around 15 research papers in various countries including India, Malaysia & Germany and has participated in around 16 FDPs, Seminars and Short-term courses. Besides this he is also serving as a potential reviewer for various internationally reputed SCI/Scopus indexed journals.